ABSTRACT

LOW-TEMPERATURE SPECIFIC HEATS
OF HEXAGONAL CLOSE-PACKED
ERBIUM-THULIUM ALLOYS

By Akella V. S. Satya

The specific heats of hexagonal close-packed erbium and thulium metals, and three of their isostructural alloys were measured in the liquid-helium temperature range between 1.3° and 4.2°K for examining the validity of the localized 4f-band model, on which the current theories of the rare-earth metals are based. Barring possible uncertainties in the magnetic properties of the samples and their impurity contents, the coefficients of the specific-heat component linear in temperature calculated from the present data range in values approximately two to twenty times the constant electronic specific-heat coefficient predicted by the above model for all the hexagonal close-packed rare-earth lanthanides. Possible explanations for such discrepancies are discussed. An itinerant 4f-band model based on the one-electron-band

model suggested by Mott is proposed for the lanthanides as an alternative to the localized 4f-band model.

LOW-TEMPERATURE SPECIFIC HEATS OF HEXAGONAL CLOSE-PACKED ERBIUM-THULIUM ALLOYS

By

Akella V. S. Satya

A THESIS

Submitted to
Michigan State University
in partial fulfillment of the requirements
for the degree of

DOCTOR OF PHILOSOPHY

Department of Metallurgy, Mechanics and Materials Science

1969

ACKNOWLEDGEMENTS

The author can express only inadequately his gratitude to Professor Chuan-Tseng Wei for suggesting this problem, his constant guidance and encouragement, and his generosity in reading the manuscript.

It is a pleasure to acknowledge his indebtedness to Professor Donald J. Montgomery, Chairman, Department of Metallurgy, Mechanics, and Materials Science, for several enlightening discussions, his constant interest, and the moral support received from him; and to Professor Austen J. Smith for many helpful discussions and valuable suggestions.

The author also wishes to extend his gratitude to Profs. Frank J. Blatt, Harold Forstat, and Carl. L. Foiles, Department of Physics, for several stimulating discussions.

Thanks are due to the National Science Foundation for making this work possible with its grant #GK-2224. It is a pleasure to acknowledge with thanks the prompt services received from the Division of Engineering

Research: its staff, the machine shop, and the electronics shop.

The close cooperation and help received in the past from Drs. Paul J. Tsang and Ram M. Srivastava are gratefully appreciated.

Finally, the author would like to acknowledge the devotion of his wife, Mrs. A. Padma Satya, who has shared with a smile all the fruitless struggles when he was attending to his earlier research problem commuting from Port Huron, Michigan, where he served as the Chief Metallurgist in the Midwest Machine Company of Indiana, Inc., for nearly two years.

TABLE OF CONTENTS

LIST OF TABLES

LIST OF FIGURES

LIST OF FIGURES (cont.)

CHAPTER I

INTRODUCTION

The physical properties and the alloying behavior of a metal depend to a large extent on the structure of its electron energy bands. Significant progress has been made in recent years in both the theoretical calculation of the energy bands and the experimental investigation of the Fermi surfaces in various metals. The electronic structure of the rare-earth metals is, however, far from being completely understood. The lanthanides, from cerium to lutetium, and the actinides, from thorium to lawrencium, together form the largest group in the periodic table, and are characterized by their partially filled f-shells in the atomic state. Even in the metallic state, the lanthanides have been traditionally viewed as consisting of trivalent atomic cores including the 4f-shell, with three conduction electrons per atom. This concept arose in an effort to explain the similarities in the chemical and the physical properties of these rare-earth metals. Any dissimilarities are attributed to the difference in the number of electrons in the 4f-shell.

Nierenberg and co-workers [1] determined the ground-state electron configurations of all the lanthanides in the atomic state, by using an atomic-beam resonance method. The results are listed in Table I-1 together with some of their physical properties.

The physical properties of the lanthanides were reviewed early by Spedding et al. [2]. Kasuya [3] treated the magnetic properties and the electrical resistivities of the lanthanides based on an s-d exchange model assuming that the atomic picture is nearly applicable for the 4f-electrons in the rare earths even in the metallic state. Yosida and Watabe [4], and Elliott and Wedgewood [5] attempted to explain some of the experimental data by assuming that only the 5d-6s electrons occupied the conduction bands, which were treated essentially as free-electron bands, perturbed perhaps by a small crystal potential.

Several calculations [6-10] for the band structure of the rare earths have appeared in the literature since then showing that the Fermi surfaces of these metals are considerably modified from those of the nearly-free-electron model. Dimmock and Freeman [6] criticized the earlier nearly-free-electron calculations [4, 5] that they failed to explain the large electronic specific heat

TABLE I-1.--Electronic configurations and some physical properties of the lanthanides

Atomic No.	Element	Atomic-state electron configurations (Ref.1)	Crystal structure	Curie temp. °K (Ref.15)	Neel temp. °K (Ref.15)	μ_f Bohr magnetons (Ref.15)	gJ Bohr magnetons (Ref.15)
57	La	$5d^1 6s^2$	hex A3'				
58	Ce	$4f^1 5d^1 6s^2$, $4f^2 6s^2$	fcc A1		12.5	0.62	2.14
59	Pr	$4f^3 6s^2$	hex A3'			0.7-1.0	3.2
60	Nd	$4f^4 6s^2$	hex A3'		7.5	2.3	3.27
61	Pm	$4f^5 6s^2$	hex A3'				
62	Sm	$4f^6 6s^2$	rhomb.		14.8		
63	Eu	$4f^7 6s^2$	bcc A2		90	5.9	7.0
64	Gd	$4f^7 5d^1 6s^2$	hcp A3	293.2		7.55	7.0
65	Tb	$4f^9 6s^2$, $4f^8 5d^1 6s^2$	hcp A3	221	229	9.34	9.0
66	Dy	$4f^{10} 6s^2$	hcp A3	85	178.5	10.2	10.0
67	Ho	$4f^{11} 6s^2$	hcp A3	20	132	10.34	10.0
68	Er	$4f^{12} 6s^2$	hcp A3	19.6	85	8.0	9.0
69	Tm	$4f^{13} 6s^2$	hcp A3	22[a]	51-60	3.4	7.0
70	Yb	$4f^{14} 6s^2$	fcc A1				
71	Lu	$4f^{14} 5d^1 6s^2$	hcp A3				

[a]Thulium-type anti-phase magnetic transformation temperature.

of gadolinium [11-13]. The specific-heat data, discussed in later sections, indicate a density of states at the Fermi surface of Gd about eight times that predicted by the free-electron model. Accurate measurements of the various properties of a screw-type spin ordering in the rare earths by Koehler et al. [14, 15] prompted Kasuya to extend his s-d exchange model [3] to incorporate the s-f interaction [16].

Dimmock and Freeman [6] calculated the band structure of gadolinium metal using the non-relativistic augmented-plane-wave (APW) approximation. Their results show that the 4f-band is only 0.05 eV wide, and is about 10.9 eV below the bottom of the conduction band, which is 5d-6s in nature. They stated that the seven localized 4f electrons per atom in gadolinium would account for the major part of the $7.5\mu_B$ saturation magnetic moment observed in this metal [17]. However, their predicted value of the electronic specific-heat coefficient of Gd is only 40% of the value measured by Lounasmaa [13], who also assumed that the three conduction electrons per atom alone occupy the hybridized 5d-6s bands. Dimmock and Freeman [6] attributed this disparity to an electron-phonon enhancement. Their representation of the density

of states of the 5d-6s conduction band at the Fermi surface is shown in Fig. 1, from which they showed that the 5d band is about 6.8 eV wide and that it resembles the d-band in the transition metals.

Based on their APW calculations Freeman, Dimmock and Watson [7] computed a Fermi Surface for the thulium metal as determined largely by the 5d band. Their Fermi-surface representation for the holes in the thulium metal is shown in Fig. 2. They agreed, however, that the position and the width of the 4f-band was strongly dependent on the periodic potential assumed. They further attempted to explain the anomalies in the temperature dependence of the resistivity [18-20] of the heavy rare earths (from Gd to Lu) in terms of the super-zone boundaries in the Fermi surface that appear as a consequence of the magnetic ordering, and found but a qualitative agreement between their theory and the experimental data. Watson, Freeman, and Dimmock [8] then considered the perturbations of the 5d bands due to the ordered 4f-moments in the heavy rare earths, and suggested that these perturbations introduced gaps in the bands largely at or near the Fermi-surface sections along its basal planes. This, they claimed,

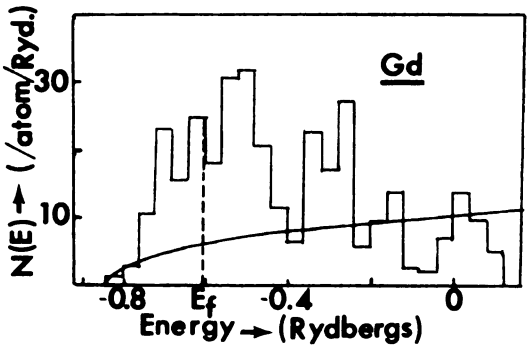

Calculated energy band for gadolinium

FIG. 1 (Ref. 6)

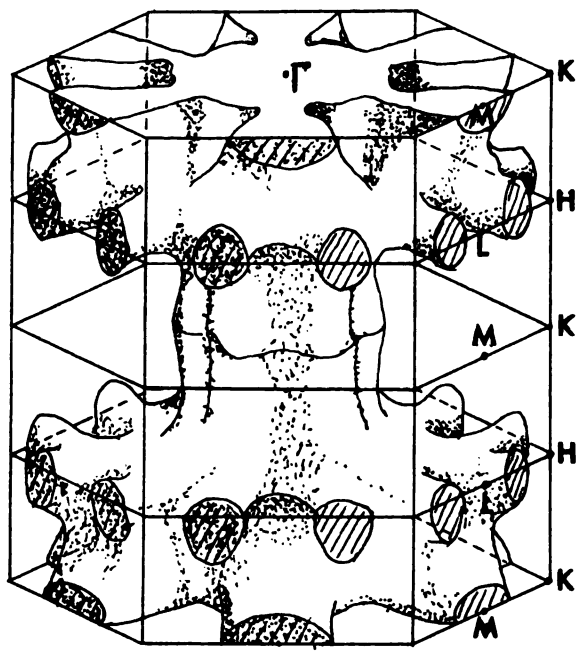

Fermi surface for holes in Tm from one-electron calculation and localized 4f-band model

FIG. 2 (Ref. 7)

destroyed or perturbed large sections of the Fermi surfaces in these metals.

Kim [9] treated the conduction electrons in the rare earths as being mediated by the exchange of spin waves with the localized spins, that might cause an enhancement in the electronic specific heat similar to that of the electron-phonon type. However, he did not bring out any quantitative comparison between his analysis and the available experimental data. Andersen and Loucks [10] calculated the band structure of bcc europium by using the relativistic APW method, and reported a density of states at the Fermi surface of 12 per atomic Rydberg. This value corresponds to an electronic specific-heat coefficient of about 0.5 milli-calorie/mole/$^{\circ}K^{2}$, which is only one-third the value obtained experimentally by Lounasmaa [13]. Andersen and Loucks [10] attributed this difference to the electron-phonon enhancement, purity of the sample, and the steepness of the density-of-states curve.

Herring [21], on the other hand, believes that there is a quite narrow group of 4f-like bands in the rare earths appreciably hybridized with the s-p-d bands. The width of this 4f-complex is presumably small compared to the energy cost of placing other than the optimum number

of 4f electrons on an atom, and only when the complex accidentally lies at the Fermi energy will there be any 4f-like portion of the Fermi surface. Herring objects the values of the widths of the 4f-like bands and their positions predicted by the one-electron calculations as being unreliable.

Considering the available Hall coefficients and the low-temperature specific-heat data Gschneidner [22] attempted to interpret the band structure of the lanthanides from an experimental standpoint. He regarded the electronic specific-heat coefficients obtained from the low-temperature data as being unreliable, and hence used the room-temperature specific-heat analysis for his treatment. He concluded that the 4f electrons occupy either discrete energy levels, or very narrow one-electron bands as proposed by Mott [23]. According to Mott [23], the overlap between incomplete 4f inner shells in the rare earths is so small that it is most unlikely that a 'metallic' type of wave function would be appropriate for the 4f electrons or that the 4f shells contribute to the Fermi surface. When the overlap between the atomic orbitals is small, an inner band would split into sub-bands of energy levels containing only one electron per atom.

The low-temperature specific heats of all the lanthanides, except Pm and Er, have been measured by Lounasmaa [24]. Similar measurements were also made by Dreyfus et al. with Pr, Sm, Tb, Ho, Er, and Tm in the temperature range of 0.4 to 4.2°K [25]. Their results were reported in a summary form only. The specific heats of Dy and Er were also reported by Parks [26]. Data of these groups are listed in Table I-2.

In analyzing the low-temperature specific-heat data, Lounasmaa [24] and Parks [26] used a localized 4f-band model such as that discussed above and assumed a more or less constant electronic specific-heat coefficient for the lanthanides of the hcp structure. Such a coefficient has often been used for comparison with the values predicted by the theoretical work.

The concept that the 4f shells in the lanthanides are partially filled and yet the 4f electrons contribute neither to the conduction band, nor to the low-temperature specific heat, is similar to the model proposed by Mott and Stevens [26] for the transition metals in which the d-electrons would be localized. Based primarily on the results of the low-temperature specific-heat work by Beck and co-workers [28], this localized d-electron model was

TABLE I-2.--Some low-temperature specific-heat data of the lanthanides

Element and crystal structure	Lounasmaa et al.[24]		Dreyfus et al.[25]	
	Gamma (millicals/mole/°K) (assumed)	Debye temp. °K (assumed)	Gamma (millicals/mole/°K)	Debye temp. °K
Ce (fcc)	5.02	147	----	---
Pr (hex)	5.83	152	4.54	85
Nd (hex)	5.38	157	----	---
Pm (hex)	----	162[a]	----	---
Sm (rhomb)	2.89	166	2.4	116
Eu (bcc)	1.37	---	----	---
Gd (hcp)	2.4	176	----	---
Tb (hcp)	2.2	181	----	---
Dy (hcp)	2.3	186	2.2	207
Ho (hcp)	2.4	191	6.2	114
Er (hcp)	--- 2.2[b]	195[a]	3.1	134
Tm (hcp)	2.5	200	5.1	127
Yb (fcc)	0.7	118	----	---
Lu (hcp)	2.7	210	----	---

[a]Interpolated values

[b]By Parks [26]

proved to be wrong and was corrected by Mott [29]. If the localized f-electron model in the rare earths is vindicated it would be a unique case in all metals.

The present work, therefore, is aimed at a study of the low-temperature specific heat of some rare-earth metals and their alloys in the hope that the results will shed some light on the nature of their band structures. The only alloy system of the lanthanides which has been investigated with the low-temperature specific-heat method is the Gd-Pr system by Dreyfus et al. [30]. They did not try to establish the localized f-electron model, but used such a model for evaluating the hyper-fine coupling constants of their alloys.

All the heavy rare-earth metals, except ytterbium, crystallize into the hexagonal close-packed structure. In the atomic state, the outer electron configurations of these lanthanides are $4f^x6s^2$, except for Gd and Lu whose configurations are respectively $4f^75d^16s^2$ and $4f^{14}5d^16s^2$. If the 4f electrons are indeed localized, and hence do not contribute to the density of states at the Fermi surface, then isostructural hcp alloys of the erbium-thulium, thulium-ytterbium, and thulium-lutetium systems should have similar Fermi surfaces as assumed by Dimmock et al.[6].

They should then reveal a constant electronic specific-heat coefficient. On the other hand, if the 4f electrons do form a band in the usual sense, and hence do contribute to the Fermi surface, then alloying thulium with erbium, which have complete solid solubility in each other, should gradually increase the number of electrons in the f band. The alloys should show variations in their electronic specific-heat coefficients.

The specific heat of a metal can be expressed as

$$C_p = C_v + C_d = C_E + C_L + C_M + C_N + C_d \qquad ...(1)$$

where C_p and C_v are the specific heats at constant pressure and volume respectively separated by the dilatation term C_d, C_E is the electronic specific heat, C_L, the lattice specific heat, C_M, the magnetic specific heat, and C_N, the nuclear hyper-fine contribution to the specific heat. The dilatation term

$$C_d = C_p - C_v = \beta^2 \eta V T \qquad ...(2)$$

where β is the volume expansion coefficient, η, the bulk modulus, and V, the volume of the sample, is negligible for solids at liquid-helium temperatures.

[3]

whe

the

Bol

whe

the

sha

whe

wit

3"(

ter

cus

Mole

According to the free-electron theory Sommerfeld [31] expressed the electronic specific heat C_E as

$$C_E = \gamma T = \frac{1}{3}\Pi^2 k^2 N(E_f) T \qquad \ldots(3)$$

where γ is the electronic specific-heat coefficient, $N(E_f)$, the density of states at the Fermi surface, and k, the Boltzman constant. Thus $N(E_f)$ is proportional to γ, and

$$N(E_f) = 1.785\ \gamma \qquad \ldots(4)$$

when γ is expressed in milli-calories/mole/$^\circ K^2$.

Stoner [32] derived a more general expression for the electronic specific heat considering an arbitrary-shaped band

$$C_E = \gamma T = \frac{1}{3}\Pi^2 k^2 N(E_f)\,[1+6kT^2 C_{N(E_f)}]\,T \qquad \ldots(5)$$

where $C_{N(E_f)} = [c_4 N''(E_f)/c_2 N(E_f)] - c_2[N'(E_f)/N(E_f)]^2 + \ldots$ with $c_2=\Pi^2/2$, $c_4=7\Pi^4/20$, $N'(E_f) = \frac{d}{dE}[N(E_f)]_{E=E_f}$, and $N''(E_f)=\frac{d^2}{dE^2}[N(E_f)]_{E=E_f}$. The implications of the $6kT^2C_{N(E_f)}$ term in the electronic specific heat expression were discussed by Tsang [33].

At low temperatures, the lattice specific heat per mole, C_L, of a simple solid can be expressed as

$$C_L = \alpha T^3 = \frac{12}{5}\Pi^4 R(T/\Theta)^3 \qquad \ldots(6)$$

according to Debye theory [34], where α is the lattice specific-heat coefficient, R, the gas constant, and Θ, the Debye characteristic temperature of the solid.

According to the spin-wave theory, the magnetic specific-heat contribution in a solid is due to the excitation of the spin waves which obey the Bose-Einstein statistics. Bloch [35] obtained the dispersion relation $\omega \propto |\bar{q}|^2$ between the general ferromagnetic spin-wave frequency ω and the wave vector $\bar{q}$. Consequently, the simple spin-wave theory [36] predicts

$$C_M = \mu T^{3/2} = c_f Nk(kT/2Js)^{3/2} \qquad \ldots(7)$$

for a ferro- or a ferrimagnet, where μ is the magnetic specific-heat coefficient, c_f, a constant depending on the crystal structure, J, the quantum mechanical exchange constant, and s, the spin-angular momentum about the z-axis. This $T^{3/2}$ dependence of the magnetic specific heat has been shown to be valid in the rare-earth garnets, Fe_3O_4, etc. [37]. For an anti-ferromagnetic material the dispersion law was found to be linear, and the magnetic specific heat was shown to be proportional to T^3 [38].

cas

ion

and

a S

of

in

whe

eff

hea

whe

nucl

Blea

rare

betw

Wher

When the nucleus of an ion has a spin, as in the case of the rare earths, the hyper-fine splitting of the ionic levels due to the mutual interaction of the nuclear and the electron dipoles comes into play, giving rise to a Schottky-type anomaly in the specific heat. At the tail of the anomaly, the Boltzmann exponential can be expanded in a power series

$$C_N/R = \sum_{n=2}^{\infty} C_n (kT)^{-n} \qquad \ldots(8)$$

where the Cn's are the various nuclear specific heat coefficients. Marshall [39] evaluated the nuclear specific heat for a ferromagnet to be

$$C_N = \nu T^{-2} = RI(I+1)A^2 s^2/3kT^2 \qquad \ldots(9)$$

where ν is the nuclear specific-heat coefficient, I, the nuclear spin, and A, the hyper-fine coupling constant. Bleaney [40] discussed the nuclear specific heat of the rare-earth metals in detail, and reported close agreement between the theory and the experiment.

Hence, in the liquid helium^{IV} temperature range, where the lattice and the nuclear specific-heat

contributions are small compared to the electronic contribution, the specific heat of the rare-earth metals and alloys can be expressed as

$$C_v = \gamma T + \alpha T^3 + \mu T^{3/2} + \nu T^{-2}. \qquad \ldots(10)$$

The present work is aimed at studying the low-temperature specific heats of the erbium and the thulium metals and their alloys in the hope that the electronic specific-heat contributions will indicate the nature of the band structure of the rare earths.

CHAPTER II

EXPERIMENTAL TECHNIQUES

Erbium and thulium metals of 99.9% purity were obtained from Messrs. Gallard Schlesinger Chemical Manufacturing Corporation in lump form. The spectrographic analyses for these metals are listed in Table II-1 together with that for the thulium samples used by Lounasmaa [24] and Dreyfus et al. [25] for comparison.

Pure erbium metal of approximately one-fifth of a mole was arc melted into two oblate-spheroid-shaped halves in a water-cooled copper crucible of an arc furnace described by Tsang [33], under a helium atmosphere. The copper crucible was cleaned with 10% nitric acid in absolute alcohol, and was repeatedly washed with pure alcohol. The crucible was then dried under vacuum, and helium gas was subsequently introduced into the furnace chamber to prevent any moisture condensation. The erbium charge was melted in two lots of about 17 grams each after evacuating and flushing the furnace chamber with helium gas for

TABLE II-1. Spectrographic analyses of the pure metals*

Element	As-received metals		Lounasmaa's	Dreyfus et al.'s
	Erbium (Lot B-7669)	Thulium (Lot B-7830)	Thulium (Ref. 24)	Thulium (private communication)
Y	0.05			
Dy	0.02	0.02		
Nd		0.05		
Yb	0.001	0.001		
Other RE's				0.01
Al	0.01	0.005	0.03	0.02
K			0.01	
Ca	0.01	0.005		0.002
Cr			0.003	
Ag				0.03
Mg	0.01	0.005	0.005	0.001
Mn			0.01	
Na			0.02	
Si	0.01	0.005		0.008
Cu	0.01			0.01
Ti			0.01	
Fe	0.04	N.D.	0.01	0.05
Ta			0.12	
O	Not determined		0.1	
N	Not determined		0.2	
C			0.014	

N.D. = Not detected. *In % by weight.

three times. The average loss of the metal due to evaporation during the melting operation was about 3%.

Because of the high vapor pressure of thulium at elevated temperatures the erbium-thulium alloys and the thulium metal sample were melted in cylindrical tungsten crucibles in an induction furnace under a purified argon

atmosphere. The induction-furnace setup is shown in Fig. 3.

The pure metals, which are easily oxidizable, were exposed to the atmosphere as briefly as possible. To minimize the contamination of the alloys by the oxygen impurity in the argon atmosphere, the gas was purified by passing over clean copper turnings held at 500°C to reduce its oxygen content to less than one part per million (partial pressure of oxygen in equilibrium with copper at 500°C is about 10^{-16} atm. [41]).

The tungsten crucibles were dried at 120°C for two hours prior to use. Referring to Fig. 5, the graphite sleeve used as a jacket for the tungsten crucibles and the refractory bricks in the induction furnace were preheated to about 1500°C prior to each melt in order to eliminate any adsorbed oxygen in the system. The furnace was then allowed to cool to room temperature under the inert atmosphere before the tungsten crucible with the charge was introduced into the furnace. The system was then closed and flushed for two hours with the purified argon gas. The charge took about twelve minutes to reach the melting point and was then maintained in the liquid state for two minutes for homogenization.

Legend for Figure 3

1 Pyrex glass window

2 Quartz tube 80 mm ϕ

3 Induction coil

4 Tungsten crucible

5 Refractory collar

6 Graphite sleeve

7 Refractory bricks

8 Silicone rubber seal
(Dow Chem. Silastic 501 RTV)

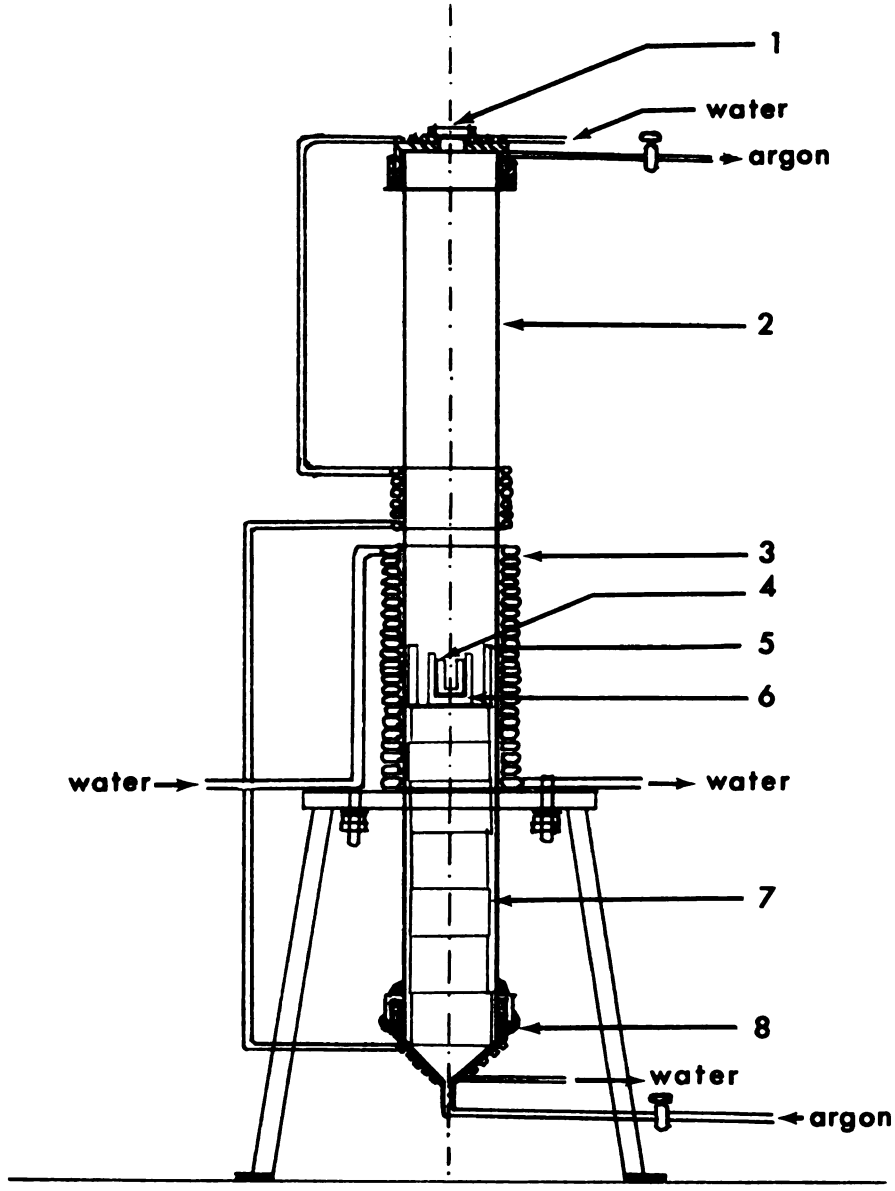

FIG. 3 Induction furnace

Dennison et al. [42] studied the amounts of tungsten and tantalum picked up by the lanthanides when the latter metals were held in either tungsten- or tantalum-crucibles at various temperatures above their melting points for an hour. They reported that about 0.1 wt% tungsten was picked up by the erbium and thulium metals when they were held molten at 50°C above their respective melting points for one hour. In view of the short time the present melts were retained in the molten state in the tungsten crucibles, it is expected that an insignificant amount of tungsten was picked up by each of these samples.

The samples were freed from the crucibles by chipping and grinding off the tungsten that might have adhered to the surface of the samples; any regions of tungsten to be removed at this stage were easily identified by a quick etch with a ½% hydrochloric acid solution. The samples were then sand-blasted to remove any surface contamination, wrapped in 0.01" thick tantalum foils, and were sealed in quartz tubes under helium at less than 10 torr. pressure. All the alloy samples were homogenized at 700°C for twenty-four hours after wrapping them in 0.01"

thick tantalum foils, and sealing them in quartz tubes under helium at less than 10 torr. pressure.

Pure thulium and three erbium-thulium alloys were induction-melted under the above conditions. Table II-2 shows their compositions as analyzed by Messrs. Atomergic Chemetals Inc. by mass-spectrographic technique after the heat-capacity measurements.

To measure the specific heat of a sample, a known quantity of heat is supplied to the sample, and the corresponding temperature rise is determined under adiabatic conditions. The heat is supplied to the sample in the form of electrical energy. The temperature of the sample is determined by measuring the resistance of a carbon resistor embedded in the specimen assembly, and the temperature rise by the change in the resistance.

The experimental setup was described by Wei [43] and by Tsang [33] except for minor modifications. As shown in Fig. 4, the apparatus consists of:

a) a cryostat for cooling the calorimeter and maintaining it at liquid-helium temperatures,

b) a low-vacuum system to lower the temperature of the liquid-helium bath from 4.2°K to 1.3°K,

TABLE II-2.--Analyses on the present melts in ppm by weight

Element	Er	$Er_{0.75}Tm_{0.25}$	$Er_{0.5}Tm_{0.5}$	$Er_{0.25}Tm_{0.75}$	Tm
Al	75	160	32	110	18
Ca	18	550	93	260	170
Ce	37	34	40	37	68
Cu	100	6	1	13	18
Dy	120	190	160	170	410
Fe	400	19	30	43	31
Ho	97	56	50	31	2
K	0.23	22	2	7	130
La	8	9	15	9	22
Mg	0.3	8	7.5	11	22
Mn	12	18	36	39	62
Na	13	3800	10	29	510
Nd	110	390	580	940	2000
Ni	3	35	46	98	600
Pr	52	42	46	24	33
Si	32	32	13	37	17
Ta	29	86	3	3	14
W	140	700	500	620	750
Y	1100	520	400	150	20
Zn	2.8	5	160	230	47
C	86	36	140	200	850
F	6300	8600	4500	3800	320
N	1300	54	21	7	1100
O	120	470	240	490	1400

c) a high-vacuum system to evacuate the calorimeter for isolating the cooled sample,

d) a manometer system and a McLeod gage to measure the vapor pressure of the liquid-helium bath, and

e) an electrical system to measure all the electrical quantities and the heating time.

A pure copper disc, shown in Fig. 5(a), was prepared to house the thermometer and the heating coil. An uncoated 1/10 watt carbon resistor was used as the thermometer. It had a nominal resistance of 56 ohms at room temperature, about 850 ohms at 4.2°K, and 50,000 ohms at 1.3°K. This thermometer was lightly greased and snugly fitted into the hole in the copper disc to provide the thermal contact between the two. The disc was then non-inductively wound with a 40-gage formex-coated manganin wire to serve as the heater. Its resistance was 325 ohms at room temperature. Both the thermometer and the heater ends were soldered to cotton-insulated 40-gage copper wires, which in turn, to 1¼" lengths of manganin leads.

Legend for Figure 4.

a) Cryostat system
b) Low-vacuum system
c) High-vacuum system
d) Manometer system
e) Electrical system
BE Bellows
C Calorimeter
CC Cold-cathode vacuum gage
CM Cathetometer
CO Counter
CV Calorimeter valve
DP Diffusion pump
FG Frequency gage
FL Fork-lift
HeC Helium gas cylinder
IP Instrument panel
K3 K-3 universal potentiometer
LHe Liquid-helium container
LN Liquid-nitrogen container
MG McLeod gage
MM Mercury manometer
NC Nitrogen gas cylinder
OM Oil manometer
OS Oscillator
P1, P2, P3, P4 Pumps
RE Recorder
SG Stokes' gage
TT Transfer tube

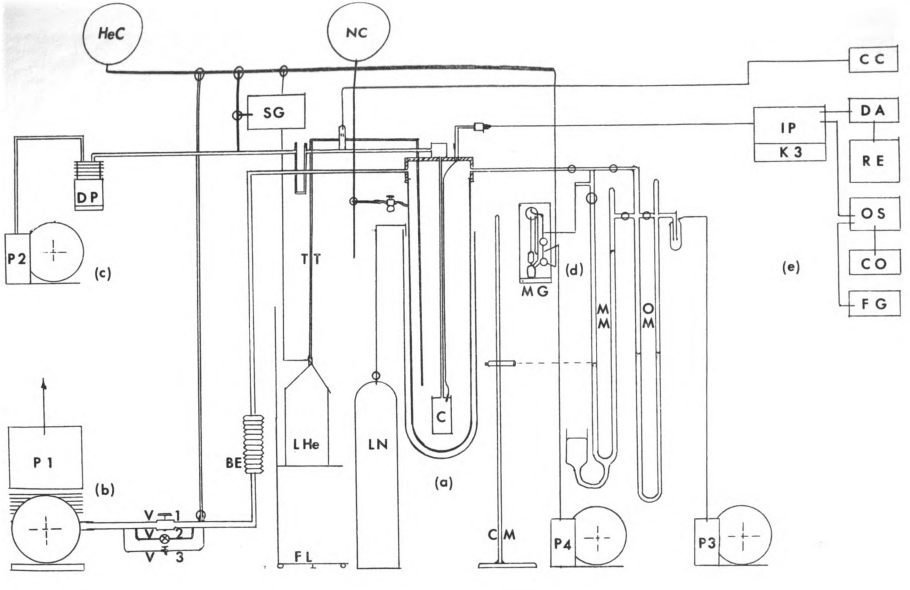

FIG. 4 Experimental setup (schematic)

Legend for Figure 5

1 Nine-pin connectors

2 Flange to high-vacuum system

3 Flange to manometer system

4 Flange to low-vacuum system

5 Protection tube

6 Middle-jacket valve MJV

7 Calorimeter conduit ½" ϕ

8 Epibond-100A seal

9 Calorimeter can

10 Lower kovar-seal connector

11 Sample

12 Heater-thermometer assembly

13 Liquid-helium cryostat

14 Liquid-nitrogen cryostat

SV Safety valve

IS Inlet screw

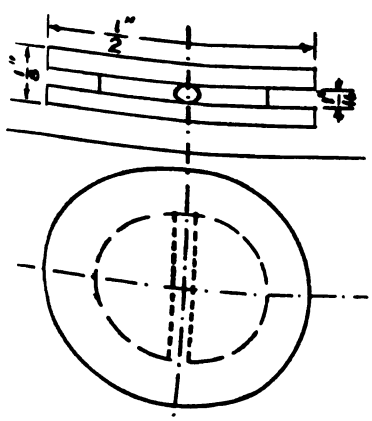

FIG. 5 (a)

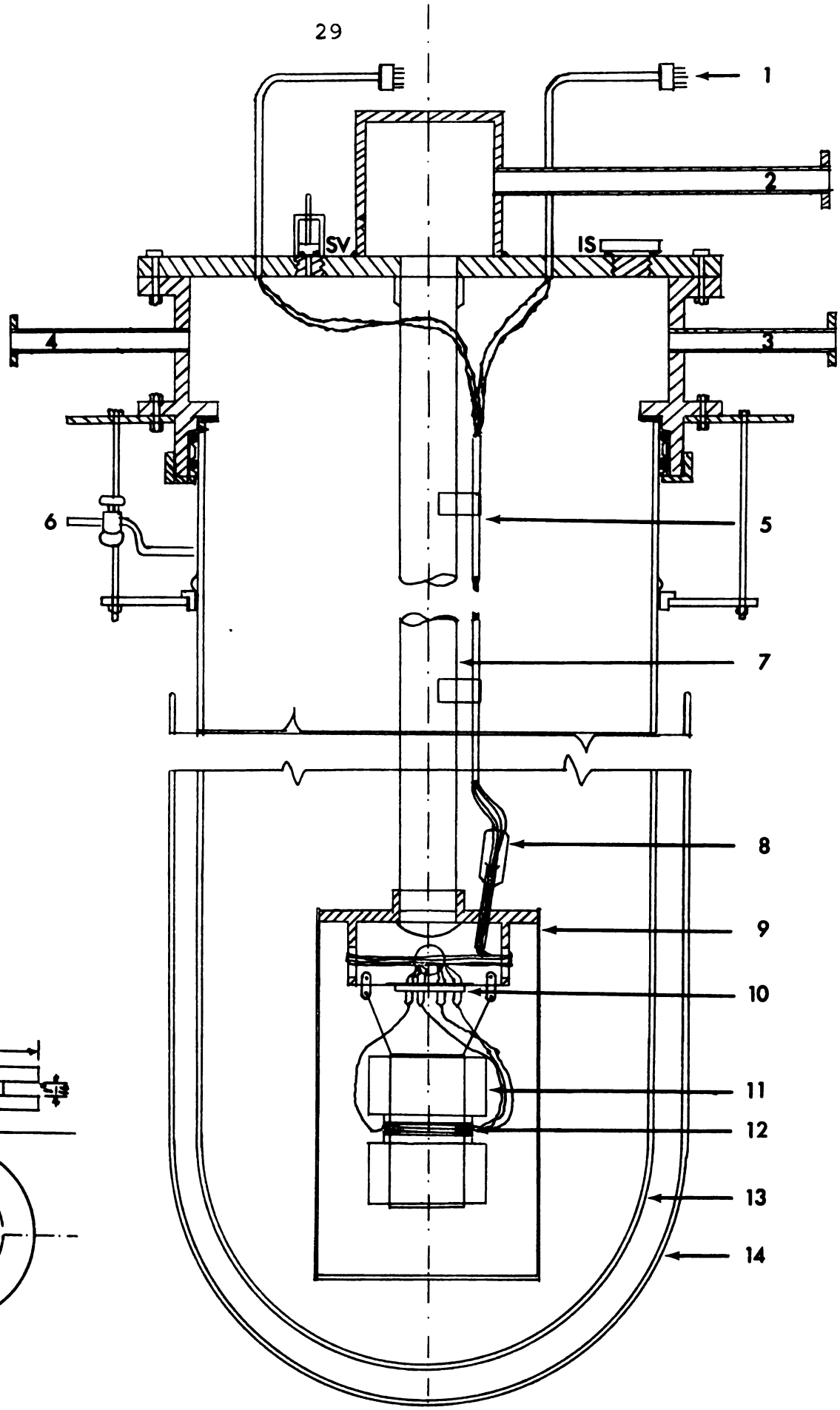

FIG. 5 Cryostat system

The sample under investigation was sliced into two cylindrical halves, and the parting surfaces were ground and polished flat to match the top and bottom surfaces of the heater-thermometer assembly. The polished surfaces were lightly greased, and the heater-thermometer assembly was sandwiched between the two sample halves and tied together with 20-gage copper wires. The assembled specimen was suspended so as to be at the center of the calorimeter can by means of three single lengths of #50 nylon thread. The lead wires from the heater-thermometer assembly were soldered to the four pins of the lower kovar seal. The electrical connections from this kovar seal to the room-temperature region at the top of the calorimeter system were also made of manganin wires. Twisted pairs of the manganin wires were taken out into the liquid-helium bath through a 1/8" copper tube, which was sealed with Epibond-100A as described by Roach et al. [44]. The heater and the thermometer wires were separated at the top of the protection tube, and were passed through two bent stainless-steel tubes, at the end of which they were soldered to two separate connectors.

The manometer system was designed to provide an accurate measurement of the vapor pressure of the liquid-helium bath from 4.2°K down to 1.3°K, by incorporating a mercury and an oil manometer, and a McLeod gage. The mercury and the oil manometers could be operated together below 50 torr., and the oil manometer and the McLeod gage, below 25 torr. The ratio of the density of mercury to that of the octoil used in the manometers was found to be 13.81. The details of this system can be seen in Fig. 6.

The resistances of the heater and the thermometer and the currents passing through them were measured by means of a Leads and Northrup K-3 universal potentiometer. The circuit diagram of the instrument panel is shown in Fig. 7, and the switch settings for the various functions are listed in Appendix A. A double-pole switch S1 was installed to activate a CMC 800A electronic counter when the heater current was turned on. The counter was connected to a Hewlett Packard 200CD audio oscillator set at 1000 cps, whose frequency was continuously checked by a separate Hewlett Packard 3734A electronic counter with a ±1 count accuracy.

Legend for Figure 6

To HeC	To helium gas cylinder
MG	McLeod gage (Todd Scientific Co.)
MM	Mercury manometer
MV1 through MV5	Manometer valves
MT	Mercury-and-oil trap
P3, P4	Mechanical fore-pumps

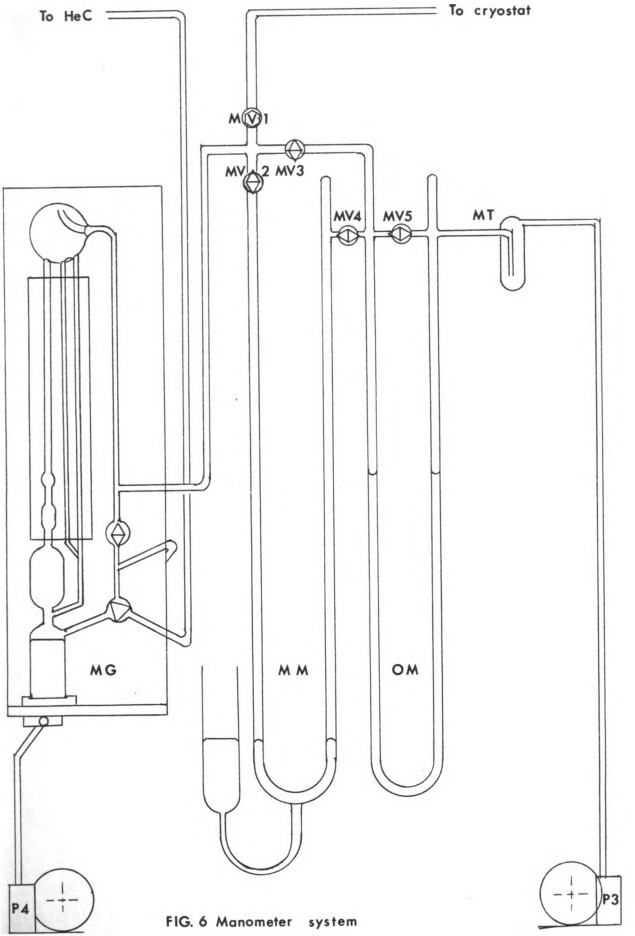

FIG. 6 Manometer system

Legend for Figure 7

BS1, BS2, BS3	Battery substitutes (constant 3-volt supply)
C1	Capacitor
CCG	Cold-cathode vacuum gage
CTR	Electronic counter
DCA	DC Amplifier
FRG	Frequency gage
MCA	Microammeter
MLA	Milliammeter
MS1	Main switch
ND	Null detector
OSC	Oscillator
P1, P2, P3, P4	Mechanical fore-pumps
R14, R16	Decade resistors for the heater and the thermometer circuits respectively
R_h, R_t	Heater resistance and thermometer resistance
REC	Recorder
RS1, RS2	Standard resistances of 100,000 and 100 ohms respectively for standardizing the thermometer and the heater currents
S1 through S19	Switches

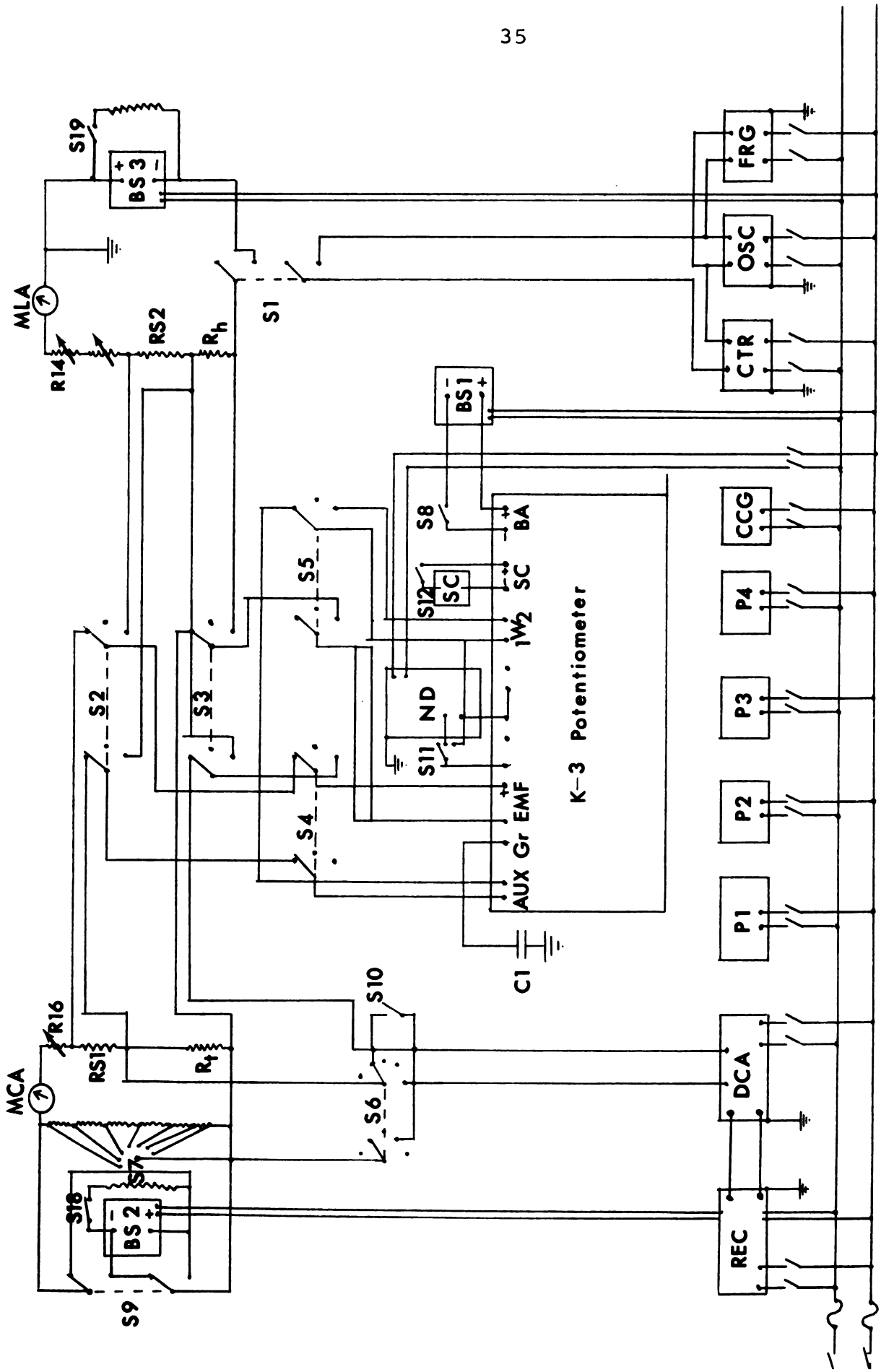

FIG. 7 Circuit diagram

The basic standard for the emf measurements with the potentiometer was a low temperature coefficient cadmium standard cell SC, which had an emf of 1.01925 volts ±0.005% at 24°C and an internal resistance of less than 500 ohms at 20°C. For current measurements, two Leeds and Northrup standard resistances RS2 and RS1 of 100 ohms ±0.005% and 100,000 ohms ±0.005% respectively were used as standards in the heating and the thermometer circuits. The accuracy of the present setup was discussed by Tsang [33]; and an over-all accuracy of ±2% can be expected in the specific-heat measurement.

The experimental procedure, as described in Appendix B, essentially involved the preparation of the cryostat for the liquid-helium transfer, the calibration of the thermometer resistance between 4.2°K and the lowest temperature attained, and the measuring of the temperature response of the thermally isolated specimen when a known quantity of heat was supplied to it.

CHAPTER III

EXPERIMENTAL RESULTS

The specific heats of the five samples described previously were successfully measured between 1.3° and 4.2°K. The calculations and the analysis of the experimental data were performed on a CDC 3600 computer. The program is given in Appendix C. The input data for the calibration were the thermometer resistance and the liquid-helium vapor pressure. Above the λ-point the vapor pressure data were corrected for the hydrostatic pressure of the liquid-helium head above the center of the calorimeter can. The temperature corresponding to the vapor-pressure values were calculated from the 1958 liquid-helium^{IV} temperature scale [45] by interpolation. The thermometer resistance and the temperature data were fitted to the Keesom-Pearlman relation [46]

$$(\log R/T)^{\frac{1}{2}} = \sum_{n=0}^{N} C_{n+1} (\log R)^n \qquad \ldots(11)$$

to yield the coefficients C_{n+1}. The calibration data from all the experiments were found to satisfy (11) with N=1

with a scatter of less than 10 milli-degrees. A typical calibration curve is shown in Fig. 8.

The specific heat of the specimen assembly consists of the contribution from the sample and that from the heater-thermometer assembly including the copper wires tieing the specimen together

$$i_h^2 R_h t/J = n_1 C_{v_1} \Delta T + n_2 C_{v_2} \Delta T \qquad \ldots(12)$$

where i_h is the heating current, R_h, the resistance of the heater, t, the heating time, J, a conversion constant to yield the energy in calories, n_1 and n_2, the number of moles of the heater-thermometer assembly and the sample respectively, C_{v_1} and C_{v_2}, their respective specific heats, and ΔT is the corresponding temperature rise. The specific heat of the sample is then

$$C_{v_2} = i_h^2 R_h t/n_2 J \Delta T - n_1 C_{v_1}/n_2. \qquad \ldots(13)$$

The heater-thermometer assembly weighed about four grams, of which the non-copper material was about 8% by weight. C_{v_1} was assumed to be that of copper with negligible error. The specific heat of copper was determined by

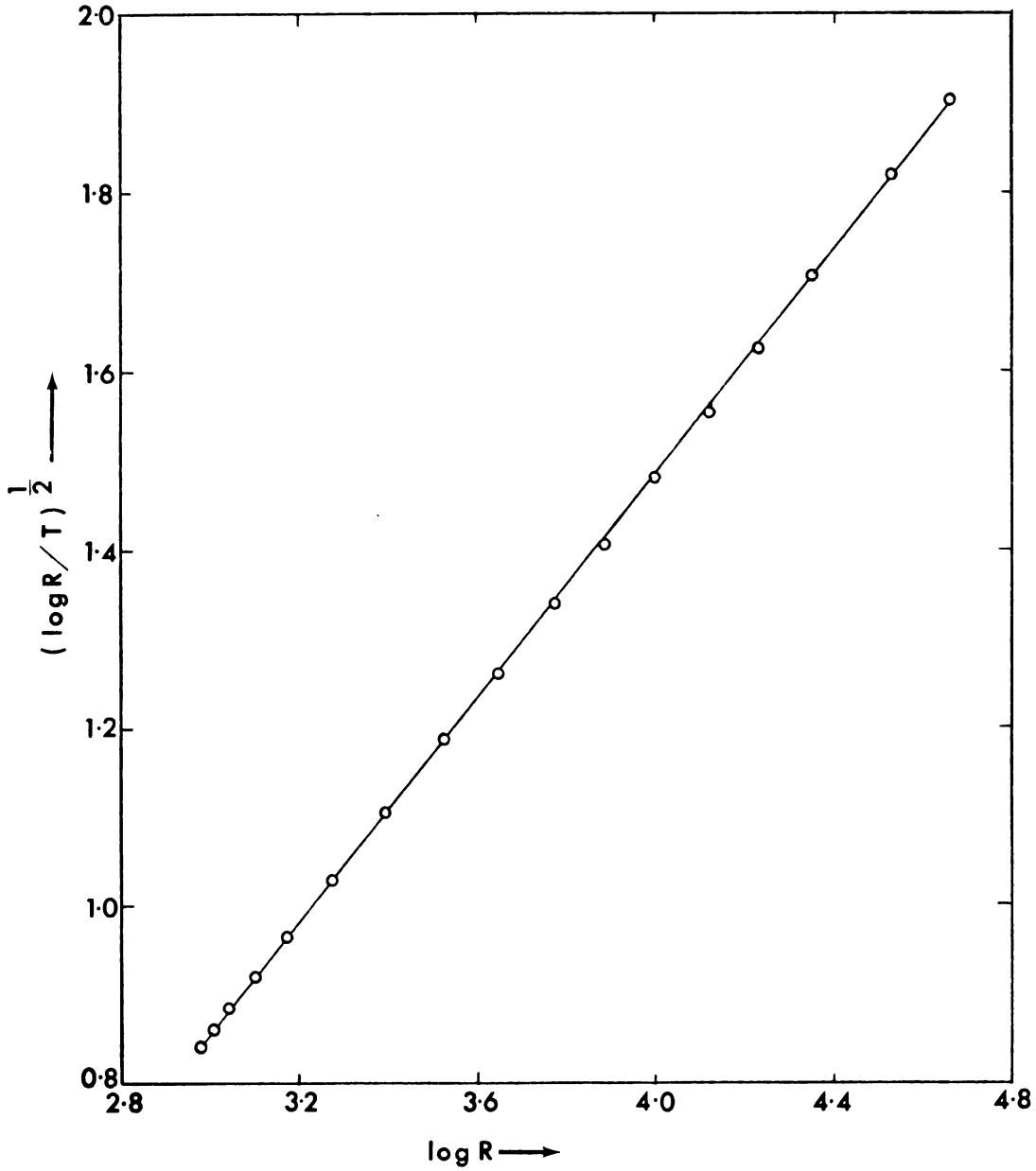

FIG. 8 Calibration for Tm

several workers and the value reported by Isaacs and Massalski [47] was

$$C_{v_l} = 0.0001668T + 0.00001159T^3 \qquad \ldots(14)$$

in calories per mole per degree K.

The five experiments were conducted with the specimens of the erbium-thulium system: two with the pure metals, and three with the alloys. The specific-heat data of the samples are listed in Tables III-1 through III-5, and the plots of the specific heat versus temperature are shown in Figs. 9 through 11.

TABLE III-1.--Specific-heat data on Erbium Sample Date: 1-31-68

Weight of sample = 31.264 gm = 0.1869185 mole.

Weight of Heater-Thermometer Assembly = 3.55 gm = 0.05587 mole.

Heater resistance at 4.2°K = 286.16, at 1.3°K = 285.95 ohms.

Thermometer-calibration coefficients: $C_1 = -1.0291935$

$C_2 = 0.6272095$

Data No.	Temperature °K	Specific Heat m-cal/mole/°K	Data No.	Temperature °K	Specific Heat m-cal/mole/°K
2	1.4213	124.86	16	2.7872	193.07
3	1.4790	124.10	17	2.9272	207.52
5	1.6379	126.76	18	3.0666	222.22
6	1.7016	130.30	19	3.2069	237.60
7	1.7545	129.49	20	3.3774	255.18
8	1.8434	135.39	21	3.4645	270.06
9	1.9803	138.86	22	3.5779	288.01
10	2.1235	147.19	23	3.7090	315.25
11	2.2437	153.76	24	3.8172	326.12
12	2.3045	156.77	25	3.8963	335.80
13	2.4144	162.00	26	3.9836	364.35
14	2.5088	171.08	27	4.1136	383.94
15	2.6807	181.96	28	4.2005	404.36

TABLE III-2.--Specific-heat data on $Er_{.75}Tm_{.25}$ alloy Date: 9-16-68

Weight of sample = 32.2917 gm = 0.192581 mole.

Weight of Heater-thermometer Assembly = 4.7821 gm = 0.07526 mole.

Heater resistance at 4.2°K = 285.755; at 1.3°K = 285.50 ohms.

Thermometer-calibration coefficients: C_1 = -1.0355476

C_2 = 0.6301181

Data No.	Temperature °K	Specific Heat m-cal/mole/°K	Data No.	Temperature °K	Specific Heat m-cal/mole/°K
1	1.3233	20.327	17	2.3500	28.052
2	1.3375	19.398	18	2.4585	30.392
3	1.3850	19.091	19	2.5889	33.637
4	1.4464	19.383	20	2.7165	37.177
5	1.4985	19.656	21	2.8758	42.432
6	1.5501	19.751	22	3.0915	50.732
7	1.5894	19.816	23	3.2297	57.325
8	1.6388	19.971	24	3.4097	65.249
9	1.6976	20.393	25	3.6295	77.270
10	1.7490	20.463	26	3.8014	87.999
11	1.8131	20.973	27	3.9177	96.319
12	1.8899	21.633	28	4.0061	102.417
13	1.9806	22.516	29	4.0755	106.604
14	2.0669	23.647	30	4.1400	111.803
15	2.1801	25.132	31	4.2023	116.161
16	2.2844	27.063			

Table III-3.--Specific-heat data on $Er_{.5}Tm_{.5}$ alloy Date: 8-2-68

Weight of sample = 28.516 gm = 0.1696401 mole.

Weight of Heater-Thermometer Assembly = 3.7255 gm = 0.05863 mole.

Heater resistance at 4.2°K = 285.955; at 1.3°K = 285.72 ohms.

Thermometer-calibration coefficients: C_1 = -1.0336623

C_2 = 0.6298109

Data No.	Temperature °K	Specific Heat m-cal/mole/°K	Data No.	Temperature °K	Specific Heat m-cal/mole/°K
1	1.3186	16.170	22	2.4275	51.617
2	1.3633	17.443	23	2.5244	56.234
4	1.4677	18.363	24	2.6431	62.883
5	1.4779	19.008	25	2.7829	71.053
6	1.5431	19.319	26	2.9257	79.876
7	1.5745	20.380	27	3.0484	87.437
8	1.6288	21.304	28	3.2234	99.597
9	1.6554	21.782	29	3.3278	104.057
10	1.6924	22.953	30	3.3917	110.607
11	1.7379	23.922	31	3.5212	120.818
12	1.7915	25.859	32	3.5992	124.213
13	1.8395	26.694	33	3.6658	130.486
14	1.8737	28.403	34	3.7299	138.970
15	1.9239	30.123	35	3.8078	140.882
16	1.9649	31.254	36	3.8674	151.890
17	2.0177	32.817	38	3.9662	154.360
18	2.0677	34.911	39	4.0227	158.044
19	2.1331	38.165	40	4.0820	164.599
20	2.2120	41.239	41	4.1261	161.679
21	2.3112	45.627	42	4.1713	175.426

TABLE III-4.--Specific-heat data on $Er_{.25}Tm_{.75}$ alloy Date: 9-11-68

Weight of sample = 32.405 gm = 0.1922968 mole.

Weight of Heater-Thermometer Assembly = 3.7715 gm = 0.05936 mole.

Heater resistance at 4.2°K = 285.755; at 1.3°K = 285.545 ohms.

Thermometer-calibration coefficients: $C_1 = -1.033711$

$C_2 = 0.630025$

Data No.	Temperature °K	Specific Heat m-cal/mole/°K	Data No.	Temperature °K	Specific Heat m-cal/mole/°K
1	1.3141	28.901	21	2.2736	64.034
2	1.3274	28.682	22	2.3518	66.011
3	1.3650	31.288	23	2.4375	69.581
5	1.4526	32.102	24	2.5623	75.066
6	1.5147	36.147	25	2.6535	75.232
7	1.5849	39.023	26	2.7662	79.628
8	1.6266	39.290	27	2.9045	83.591
9	1.6605	41.355	28	3.0392	85.571
10	1.6899	41.941	29	3.1746	88.834
11	1.7248	43.516	30	3.3366	90.022
12	1.7702	45.091	31	3.4848	96.076
13	1.7945	44.544	32	3.5951	100.006
14	1.8282	46.391	33	3.6627	97.744
15	1.8664	47.644	34	3.7635	101.249
16	1.9137	50.714	35	3.8573	104.191
17	1.9665	50.879	36	3.9396	104.422
18	2.0244	54.079	37	4.0140	103.868
19	2.1030	51.475	38	4.0979	106.948
20	2.1742	60.119	39	4.1631	107.394

TABLE III-5.--Specific-heat data on Thulium sample Date: 8-22-68

Weight of sample = 27.094 gm = 0.16038216 mole.

Weight of Heater-Thermometer Assembly = 3.8885 gm = 0.061198 mole.

Heater resistance at 4.2°K = 285.805; at 1.3°K = 285.585 ohms.

Thermometer-calibration coefficients: $C_1 = -1.0341672$

$C_2 = 0.6297254$

Data No.	Temperature °K	Specific Heat m-cal/mole/°K	Data No.	Temperature °K	Specific Heat m-cal/mole/°K
1	1.3029	19.121	18	2.3697	38.042
2	1,3155	19.574	19	2.4944	40.446
3	1.3658	20.496	20	2.5822	42.779
4	1.4127	20.827	21	2.7223	45.484
5	1.4710	21.904	22	2.8829	49.550
6	1.5233	22.601	23	3.0107	52.650
7	1.5807	23.210	24	3.1418	56.157
8	1.6244	24.296	25	3.2995	60.480
9	1.6744	24.790	26	3.5023	66.401
10	1.7448	25.937	27	3.6824	72.241
11	1.8185	27.099	28	3.8105	76.917
12	1.8777	28.320	29	3.8845	79.329
13	1.9258	29.244	30	3.9542	82.633
14	1.9853	30.356	31	4.0284	83.291
15	2.0479	31.622	32	4.0896	84.370
16	2.1210	32.692	33	4.1547	86.619
17	2.2242	35.013	34	4.2175	91.545

200

15

Specific heat (milli cals/mole/°K)

1

FIG.

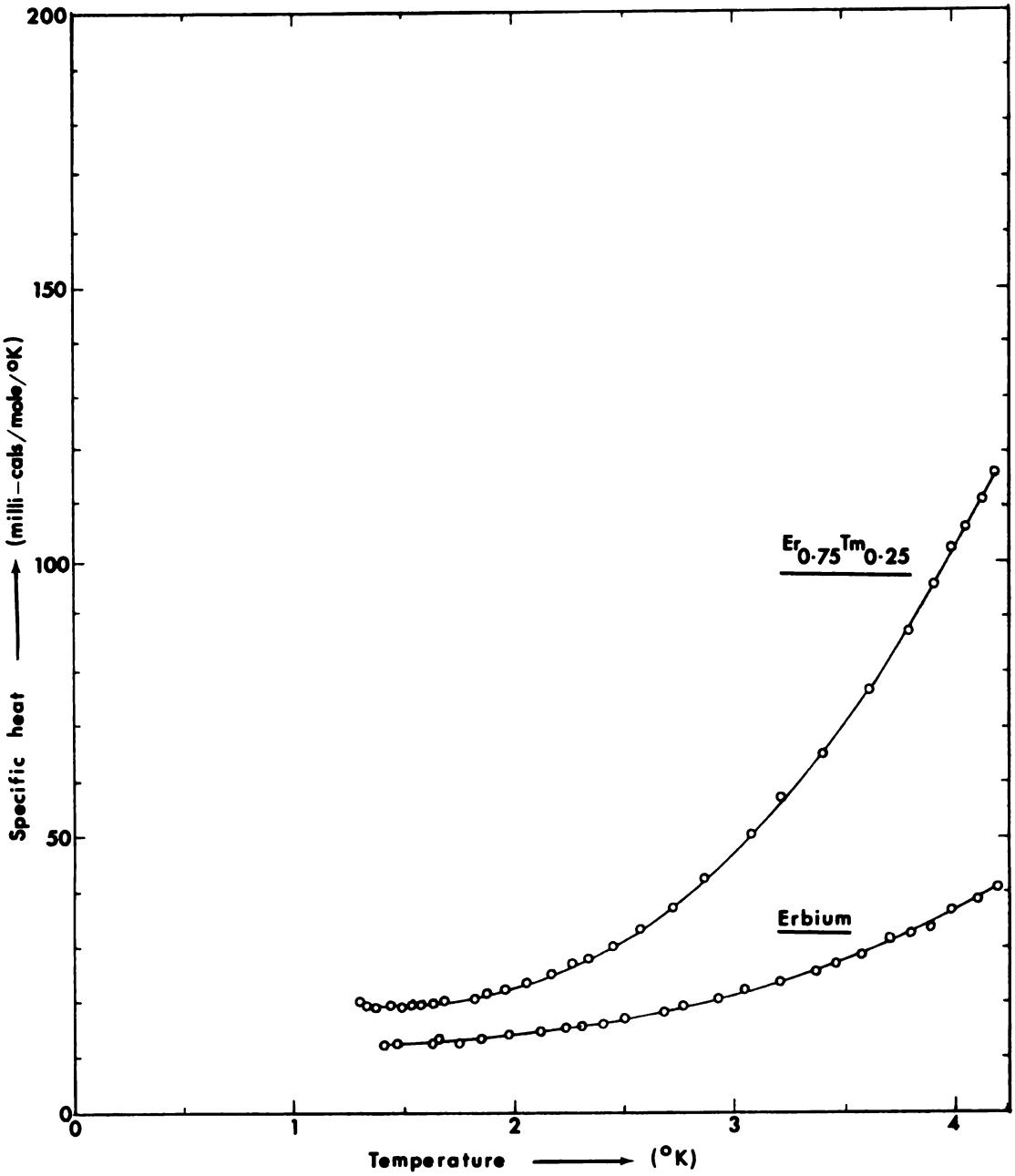

FIG. 9 Specific heat vs. temperature curve for Er and $Er_{0.75}Tm_{0.25}$

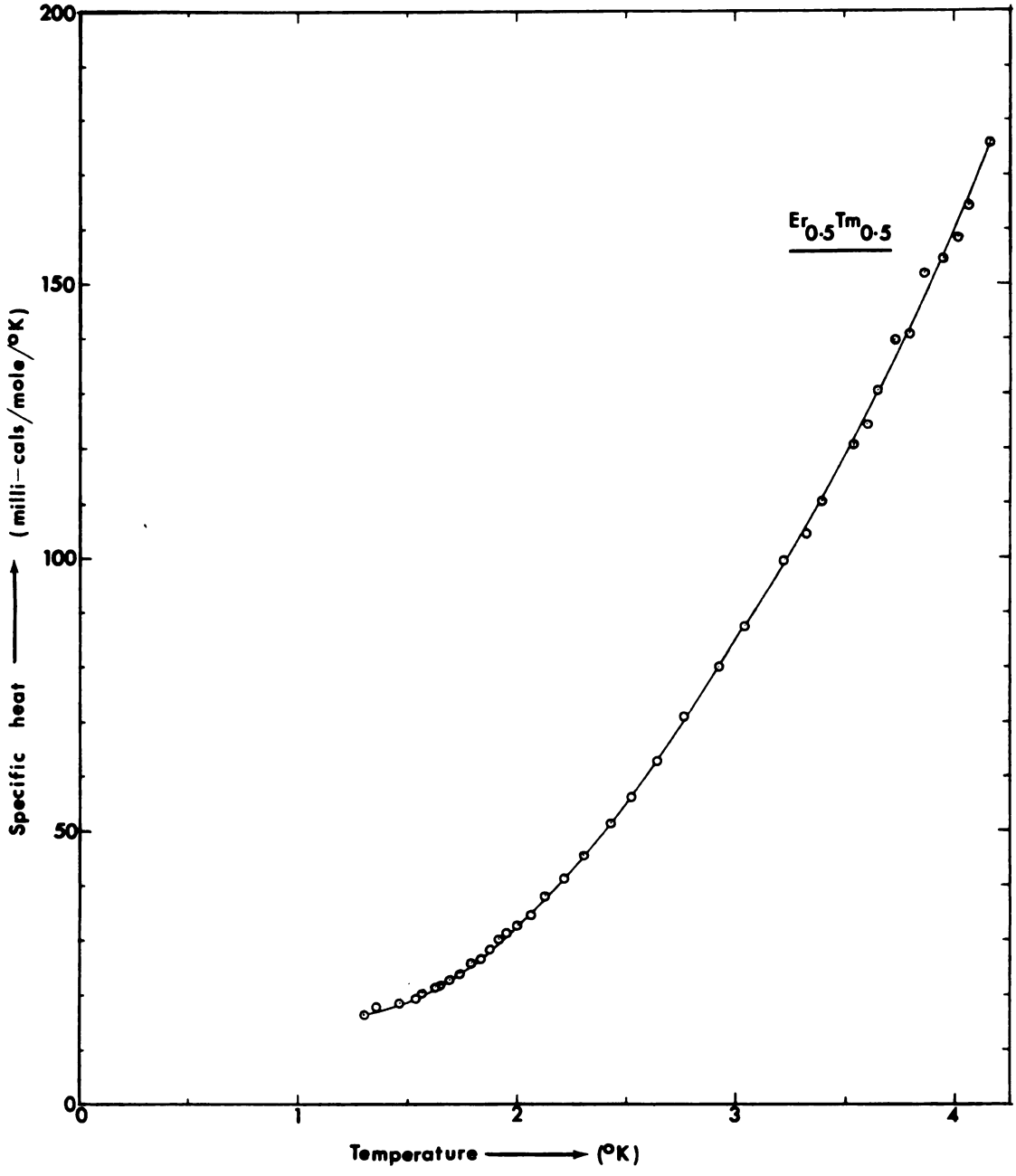

FIG. 10 Specific heat vs. temperature curve for $Er_{0.5}Tm_{0.5}$

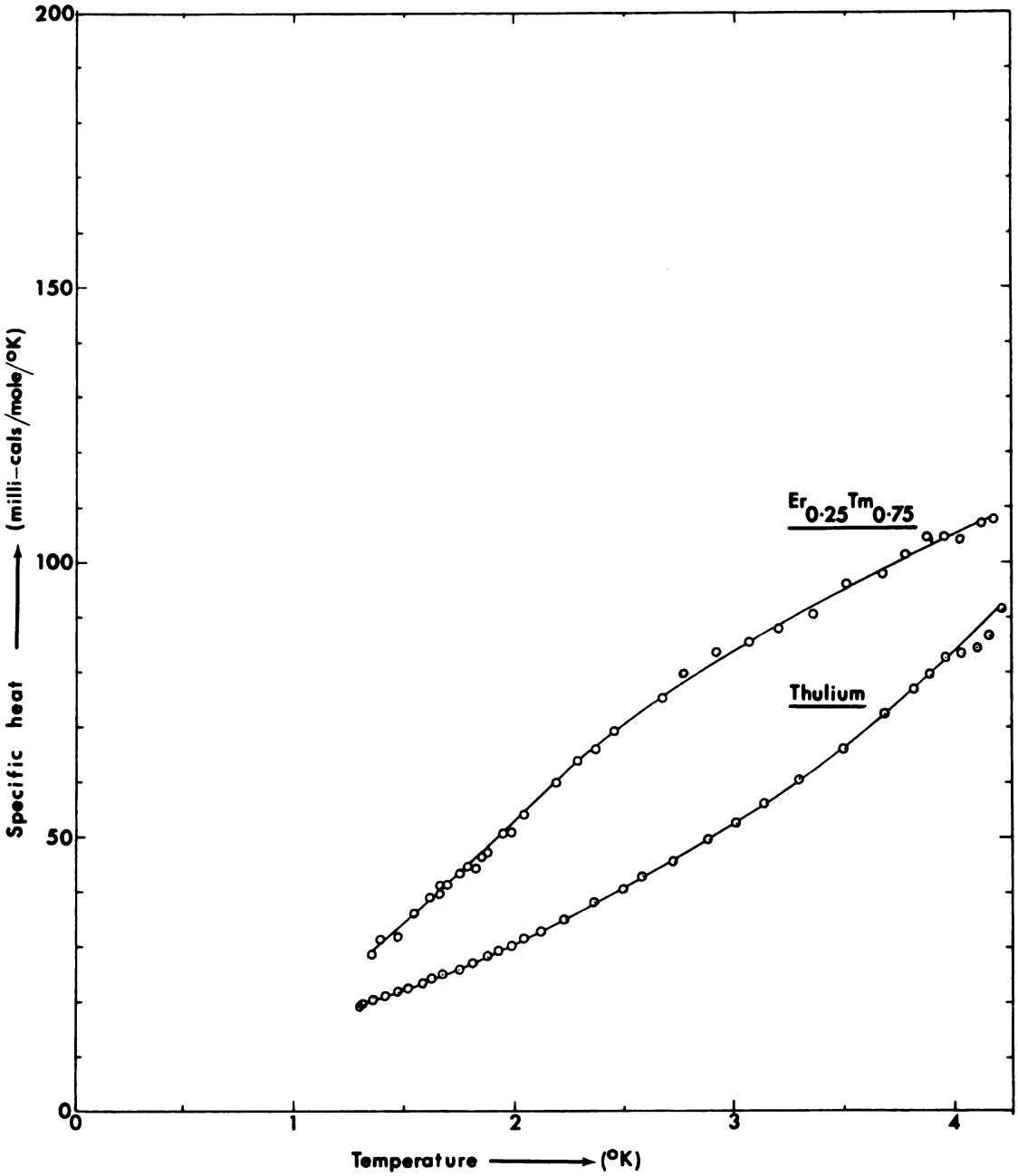

FIG. 11 Specific heat vs. temperature curve for $Er_{0.25}Tm_{0.75}$ and Tm

CHAPTER IV

DISCUSSION

The specific-heat data on erbium, thulium, and their alloys were given in the preceding chapter. A proper analysis of these data for the separation of the various specific-heat contributions as discussed in Chapter I depends on a knowledge of the magnetic properties of the specimens under investigation.

Koehler and co-workers [14] studied the magnetic properties of the rare-earth elements by neutron-diffraction techniques. They found that erbium transformed from its high-temperature antiphase structure into a ferro-magnetic spiral configuration at its Curie temperature T_c of 19.6°K with the basal components retaining their helical arrangements. The resultant magnetic moment lies on the surface of a cone generated around the c-axis. The half apex angle θ of the cone was found to change with temperature.

Koehler [15] also found that thulium adopted an antiphase domain-type structure below its Curie temperature of 40°K, in which four layers of north-pointing moments

were followed by three layers of south-pointing moments. The period of this magnetic structure was noted to be constant at seven layers over the temperature range. At 4.2°K each thulium atom had its maximum moment of 7.0 μ_B, parallel or antiparallel to the c-axis. Because of the incomplete cancellation, there was a net moment of 1.0 μ_B per atom parallel to the c-axis. These low-temperature magnetic structures of erbium and thulium are shown in Fig. 12, and their measured magnetic moments are compared with the ground state values gJ predicted from the Hund's rule in Table I-1.

Bozorth and Gambino [48] studied the magnetic properties of the solid solutions of several heavy rare earths. They noticed a maximum in the Curie temperatures at 40% Er in the erbium-holmium system. In the Er-Tm system they found that the Curie temperature decreased with increasing thulium content up to about 12% Tm as shown in Fig. 13. At this point there was a jump in the curve, and the new Curie temperature Tc_2 followed a slowly declining trend again with increasing thulium content. This Tc_2 was suggested to be the thulium-type Curie temperature, below which the saturation magnetization is very low due to the antiphase domain-type of magnetic ordering.

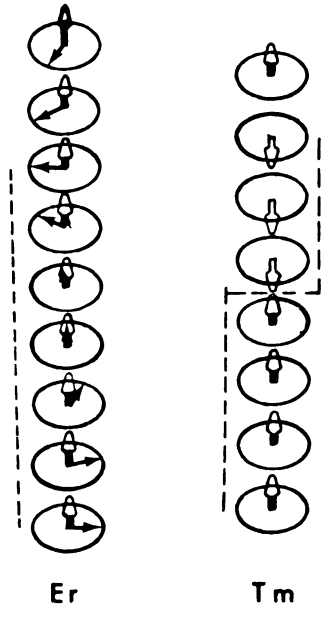

FIG. 12 Low-temperature magnetic structures of Er and Tm

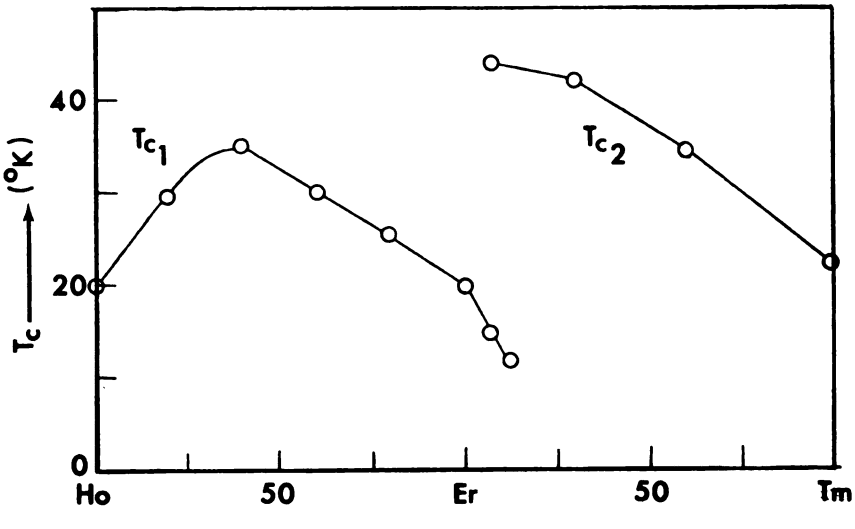

FIG. 13 Curie temp. vs. composition for Ho-Er and Er-Tm systems

Lounasmaa [49] studied the specific heat of several rare-earth metals also in the 3 to 25°K temperature range mainly to analyze the magnetic specific heat C_M. He found that the magnetic specific heat of thulium was 1.5 $T^{2.5}$ milli-cals/mole/°K in the 0.4 to 4°K temperature range, and 1.98 $T^{2.3}$ milli-cals/mole/°K in the 4 to 20°K range in contrast to the $T^{3/2}$ dependence predicted by the spin-wave theory for the ferri- and ferromagnetic materials, and the T^3 dependence for the antiferromagnets. Lounasmaa attributed the differences between his results and the theoretical predictions to the lack of validity of the existing theory to the antiphase magnetic structure such as that of thulium. One may, however, note the apparent closeness of the experimentally analyzed magnetic specific heat values of thulium to that predicted by the spin-wave theory for the antiferromagnetic structure.

In the case of holmium metal, which also has a ferromagnetic spiral type of structure similar to erbium below its Curie point of 20°K, Lounasmaa [49] obtained C_M=0.36 $T^{3.2}$ milli-cals/mole/°K in the 3 to 20°K temperature range, and a T^3 dependence for C_M in the 0.4 to 4.2°K range. Kaplan [50] suggested that for a ferromagnetic spiral structure the dispersion relation between $\omega(\underline{q})$ and

$\underline{q}$ was linear for small values of the wave vector $\underline{q}$ even though the net spin was not zero. This dispersion relation, similar to that deduced for the antiferromagnetic case, was attributed to the normal modes corresponding approximately to oscillations of the components perpendicular to the magnetization. These components themselves formed an antiferromagnetic spiral. From this interpretation, Kaplan [50] treated the ferromagnetic-spiral structure as being similar to that of an antiferromagnet, the magnetic specific-heat contribution of which was proportional to T^3 as noted in Chapter I.

From the foregoing discussion, one may expect a T^3 dependence of the magnetic specific heat for all the present samples. The specific-heat data on erbium, thulium, and their alloys, as presented in Tables III-1 through III-5, were therefore analyzed with

$$C_v/T = \gamma + (\alpha+\mu)T^2 + \nu T^{-3}. \qquad \ldots(15)$$

Since the aim of the present work is to examine the validity of the localized 4f-band model, no assumption was made on the nature of the 4f band.

The main computer program was written to analyze the present specific-heat data to obtain the electronic, lattice plus magnetic, and the nuclear specific-heat contributions according to equation (15). To analyze the magnetic term, the nuclear and the lattice specific-heat contributions were subtracted from the total specific heat, and the electronic and the magnetic contributions were easily separated from the remainder. The lattice specific heat was calculated from the Debye temperatures taken from Lounasmaa's work [24].

The analysis, as outlined above, is straightforward for the specific-heat data of the erbium, $Er_{0.75}Tm_{0.25}$, and the thulium samples. The $Er_{0.5}Tm_{0.5}$ and $Er_{0.25}Tm_{0.75}$ samples, however, offer some difficulty. As shown in figures 16 and 17, the C_v/T versus T^2 curves for these samples appear to be concave downwards in the middle similar to that for $Gd_{0.23}Pr_{0.77}$ in the work of Dreyfus et al. [29]. None of the known theories seem to be able to account for such a feature. In order to obtain an upper and a lower limit for the electronic specific-heat coefficient, the C_v/T data of the $Er_{0.5}Tm_{0.5}$ sample was analyzed by first fitting the values below 2.5°K to equation (15) to evaluate

the nuclear contribution, which was then subtracted from the C_v/T values for the entire temperature range. The remainder, consisting of only the linear and the T^3 terms in C_v, was analyzed by treating separately the data below and above 2.78°K for $\gamma_{min.}$ and $\gamma_{max.}$ respectively. The true electronic specific-heat coefficient would probably lie between these two values. For the $Er_{0.25}Tm_{0.75}$ sample, $\gamma_{min.}$ and $\gamma_{max.}$ were obtained by extrapolating the two branches of the C_v/T curve to 0°K.

Figures 14 through 18 show the results of the analysis. The various specific-heat coefficients are listed in Table IV-1, while the electronic specific-heat coefficients are plotted against the composition in fig. 19.

TABLE IV-1.--Specific-heat contributions of the present samples in milli-cal/mole/°K

Sample	Electronic	Lattice	Magnetic	Nuclear
	T	T^3	T^3	T^{-2}
Erbium	4.1T	$0.063T^3$	$1.23T^3$	$11.73T^{-2}$
$Er_{0.75}Tm_{0.25}$	2.5T	$0.0615T^3$	$1.4T^3$	$23.9T^{-2}$
$Er_{0.5}Tm_{0.5}$	$8.7\pm5.3T$	$0.060T^3$	$2.4\pm0.8T^3$	$9.29T^{-2}$
$Er_{0.25}Tm_{0.75}$	$23.3\pm7.87T$	$0.059T^3$	----	----
Thulium	13.3T	$0.058T^3$	$0.42T^3$	$1.76T^{-2}$

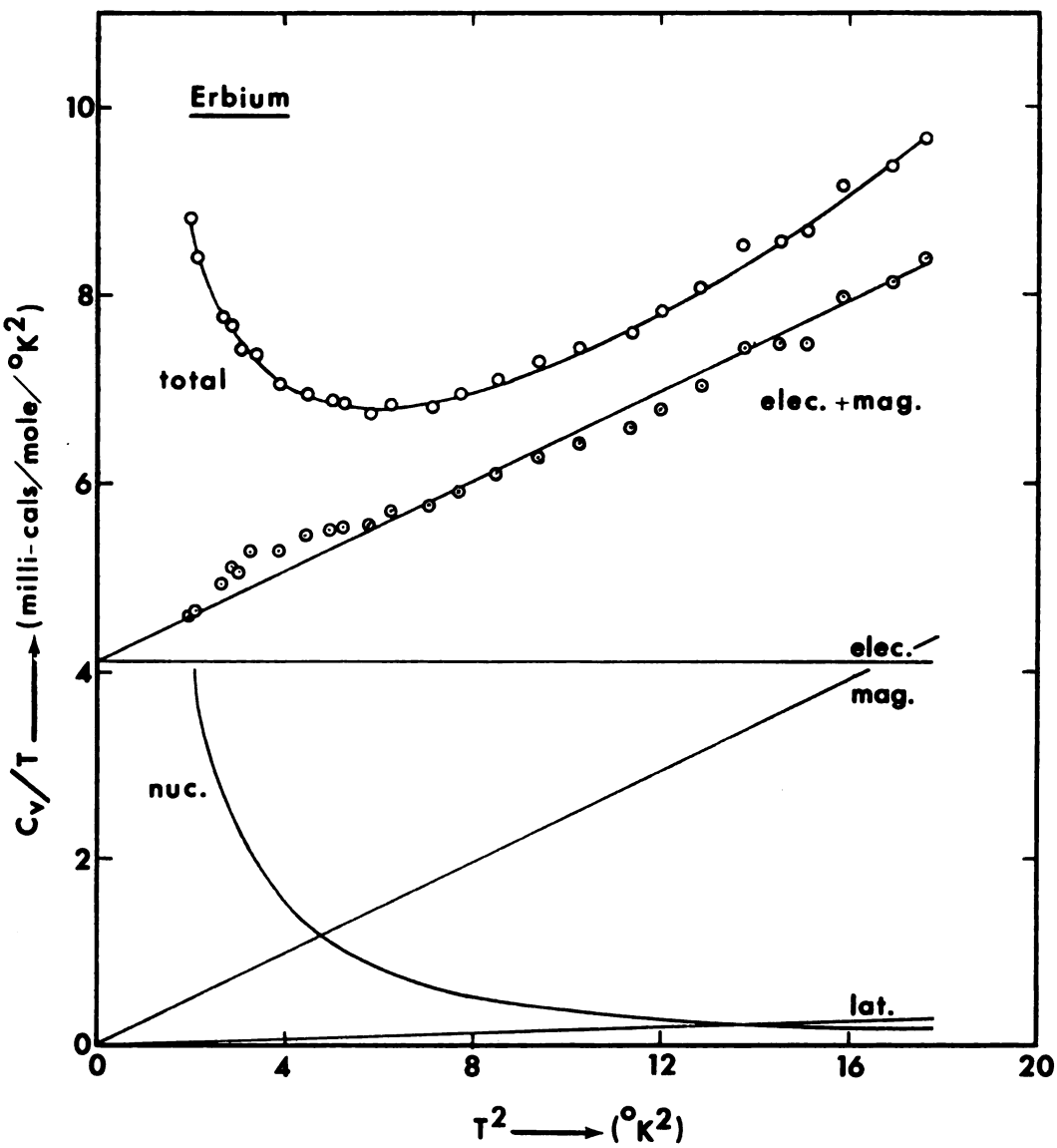

FIG. 14 C_v/T vs. T^2 curves and analyses for Er


C/T ⟶ (milli cals/mole/°K²)

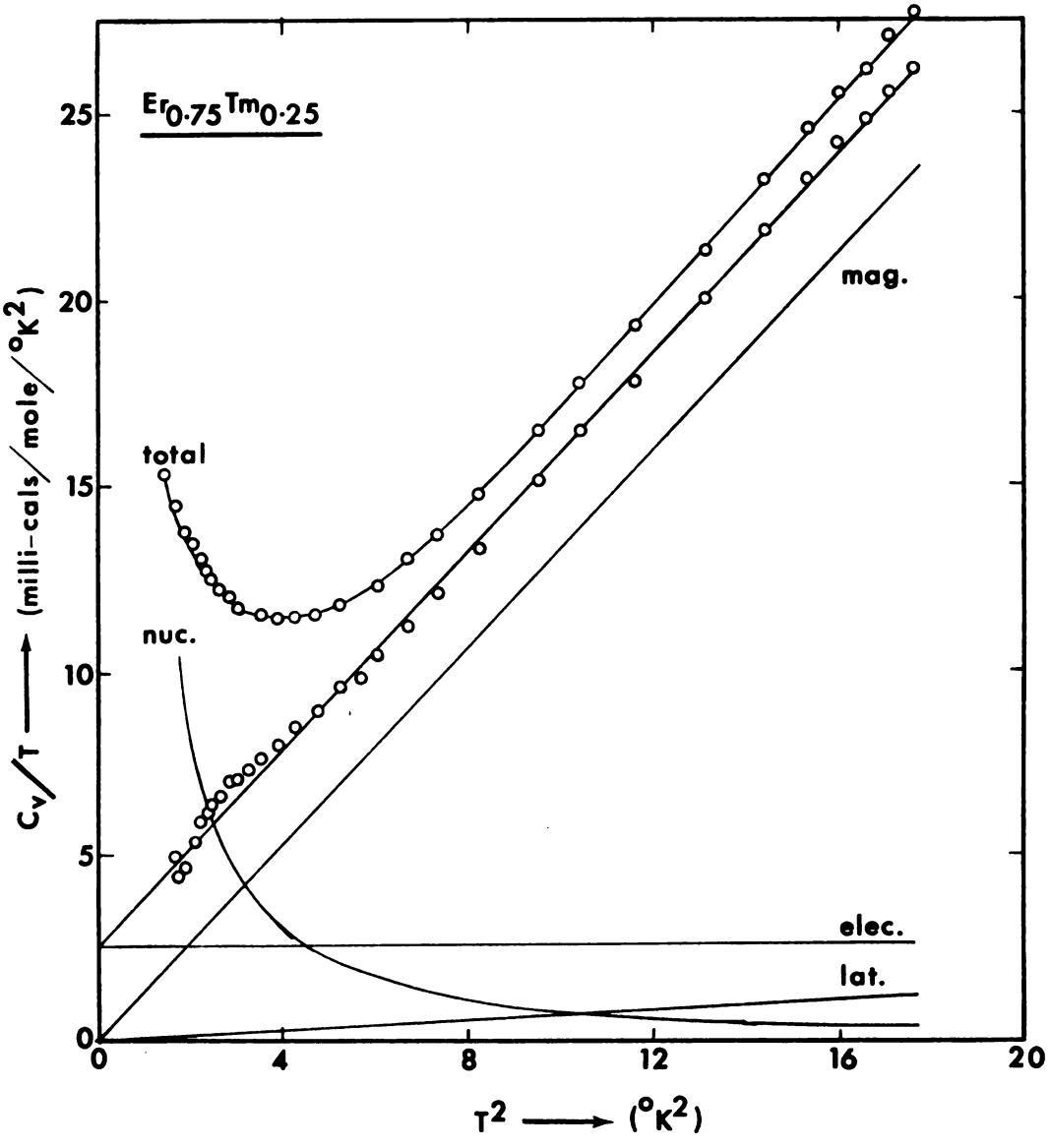

FIG. 15 C_v/T vs. T^2 curves and analyses for $Er_{0.75}Tm_{0.25}$

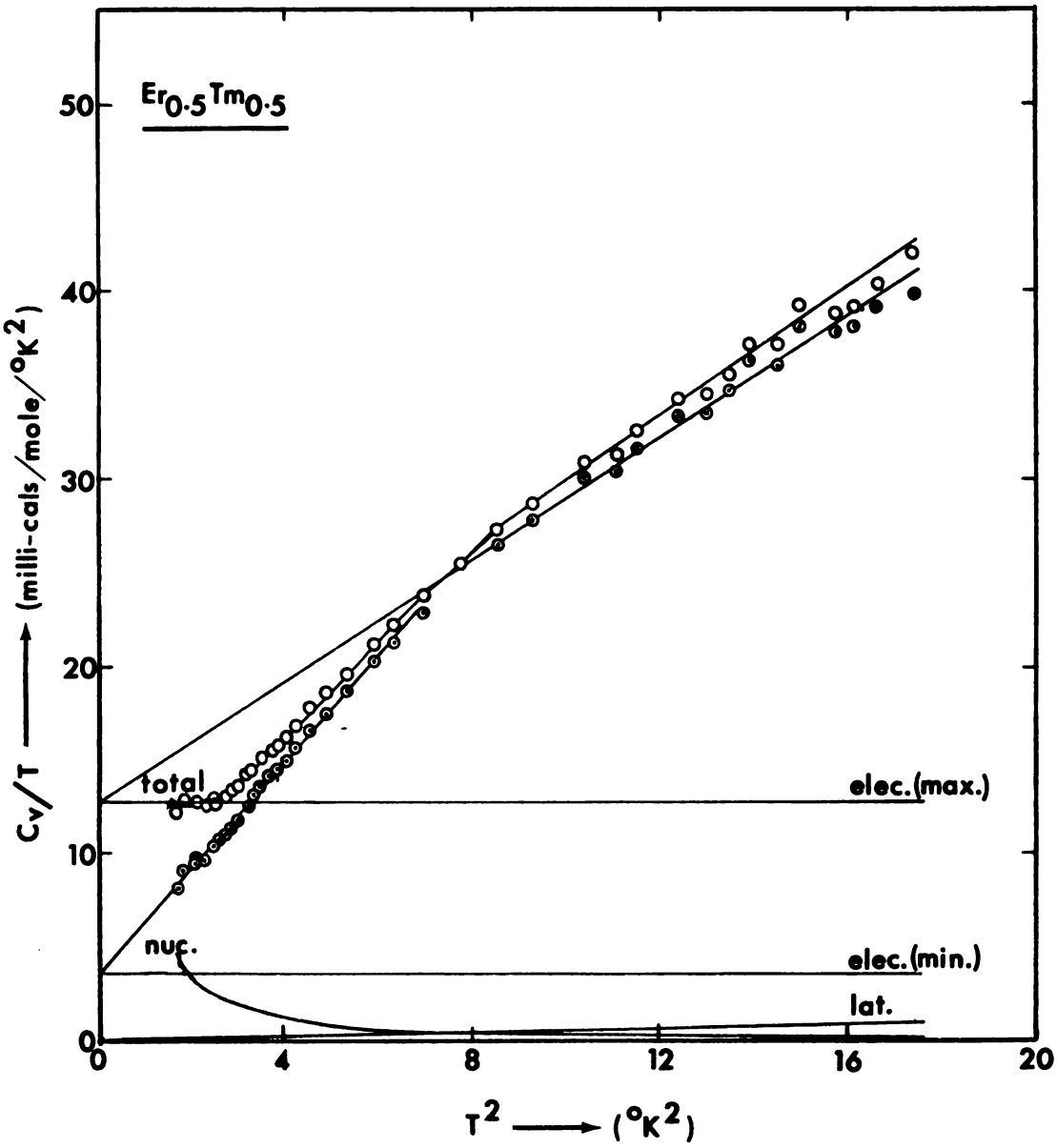

FIG. 16 C_v/T vs. T^2 curves and analyses for $Er_{0.5}Tm_{0.5}$

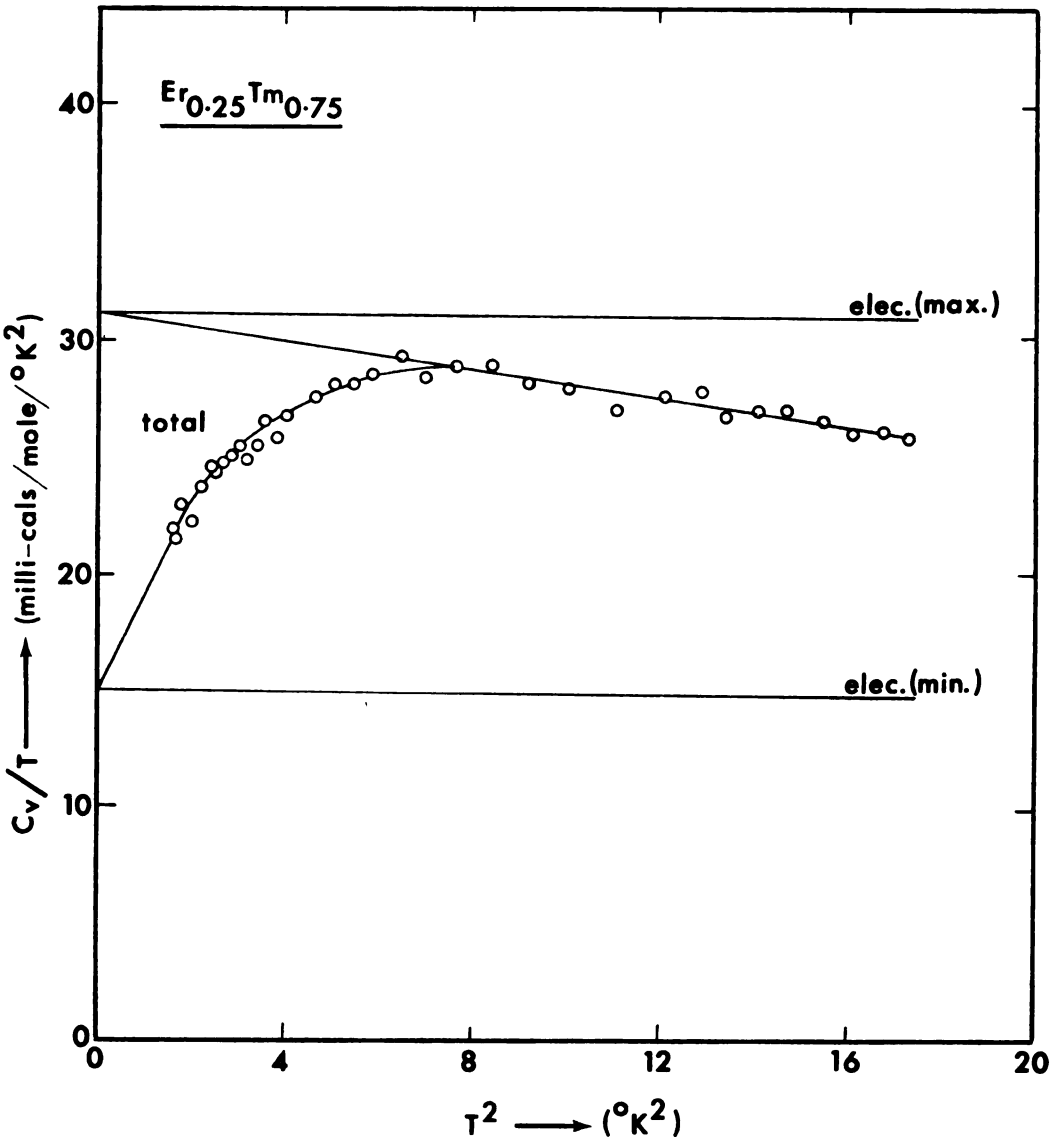

FIG. 17 C_v/T vs. T^2 curves and analyses for $Er_{0.25}Tm_{0.75}$

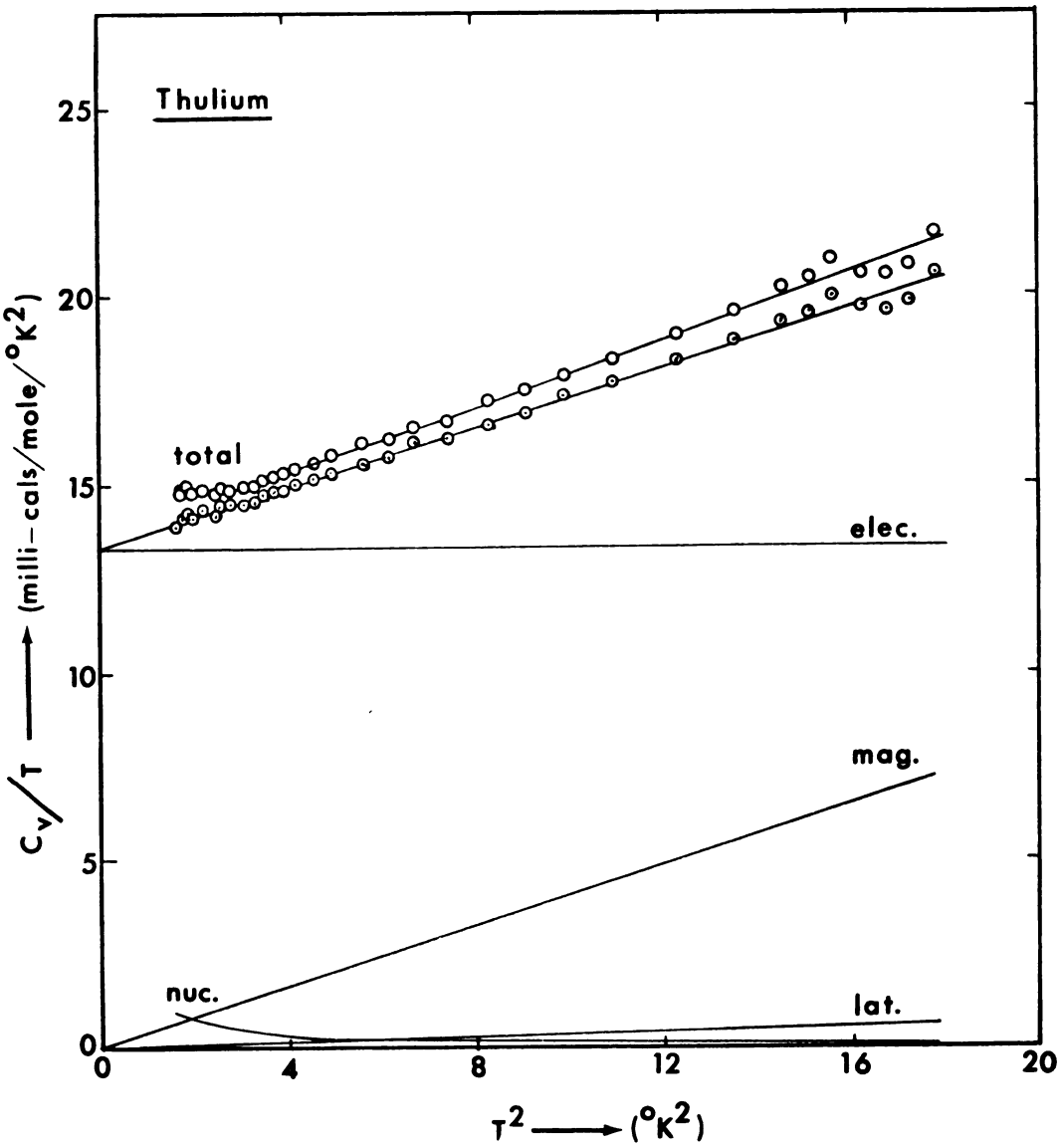

FIG. 18 C_v/T vs. T^2 curves and analyses for Tm

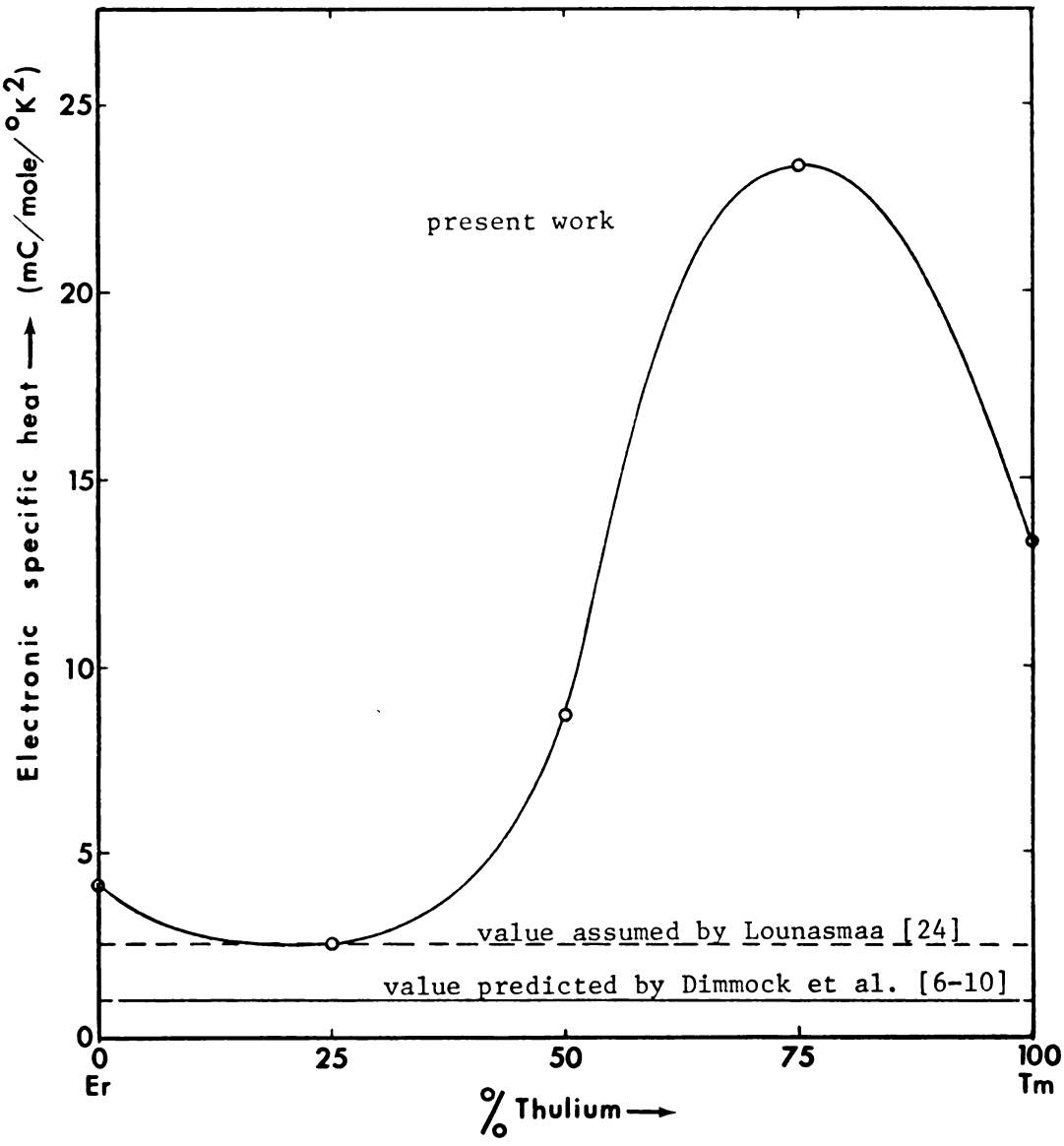

FIG. 19 Electronic specific-heat coefficient vs. % Tm

The results indicate that the γ values of the samples range from 2.5 to 23 ± 8 milli-cals/mole/$^{\circ}K^2$. Figure 19 also shows, for comparison, the constant value of 1 milli-cal/mole/$^{\circ}K^2$ predicted by the APW-calculations of Dimmock et al. [14-18], and the nearly constant value of about 2.5 milli-cals/mole/$^{\circ}K^2$ assumed by Lounasmaa [24], both based on the localized 4f-band model. Although the differences between the theoretically predicted value and the experimentally obtained electronic specific-heat data [24, 25] for the rare earths are not entirely new, the present data indicate that the difference can be much greater for some of the alloys. The discrepancies have been so far attributed to the electron-electron enhancement [9], the electron-phonon [10] and electron-magnon enhancements [16], and the impurity contents in the samples of the different workers [10]. Kasuya [16] estimated an electron-phonon enhancement of about 30% and an electron-magnon enhancement of about 20% of the γ value for gadolinium. These enhancements can account for at most a factor of two.

The low-temperature specific heats of erbium and thulium reported by different workers are compared in

Fig. 20 with the present data. Lounasmaa [24] pointed out that discrepancies in the specific heats of such magnitudes are not uncommon below 4°K for the rare earths. He attributed the discrepancies to the differences in the impurity contents in the samples.

The effect of oxygen in gadolinium on its specific heat was investigated by Crane [51]. He reported an increase in the specific heat with increasing amounts of oxygen. This effect was explained in terms of the magnetic ordering of the Gd^{+} ions in the oxide. No specific-heat measurements on erbium and thulium oxides have been reported. If a quantitative analogy could be assumed between the effects of oxygen on the specific heats of Gd and the Er-Tm alloys, about 0.1% oxygen by weight might cause an enhancement in the specific heats by as much as a factor of two. With all the effects contributing to the uncertainties in the measured γ values taken into consideration, a factor of not exceeding four can be included in the corrections. This is still insufficient to bring down the γ values of the thulium, $Er_{0.5}Tm_{0.5}$, and $Er_{0.25}Tm_{0.75}$ samples to the 1 milli-cal/mole/$°K^2$ range predicted by the localized 4f-band model.

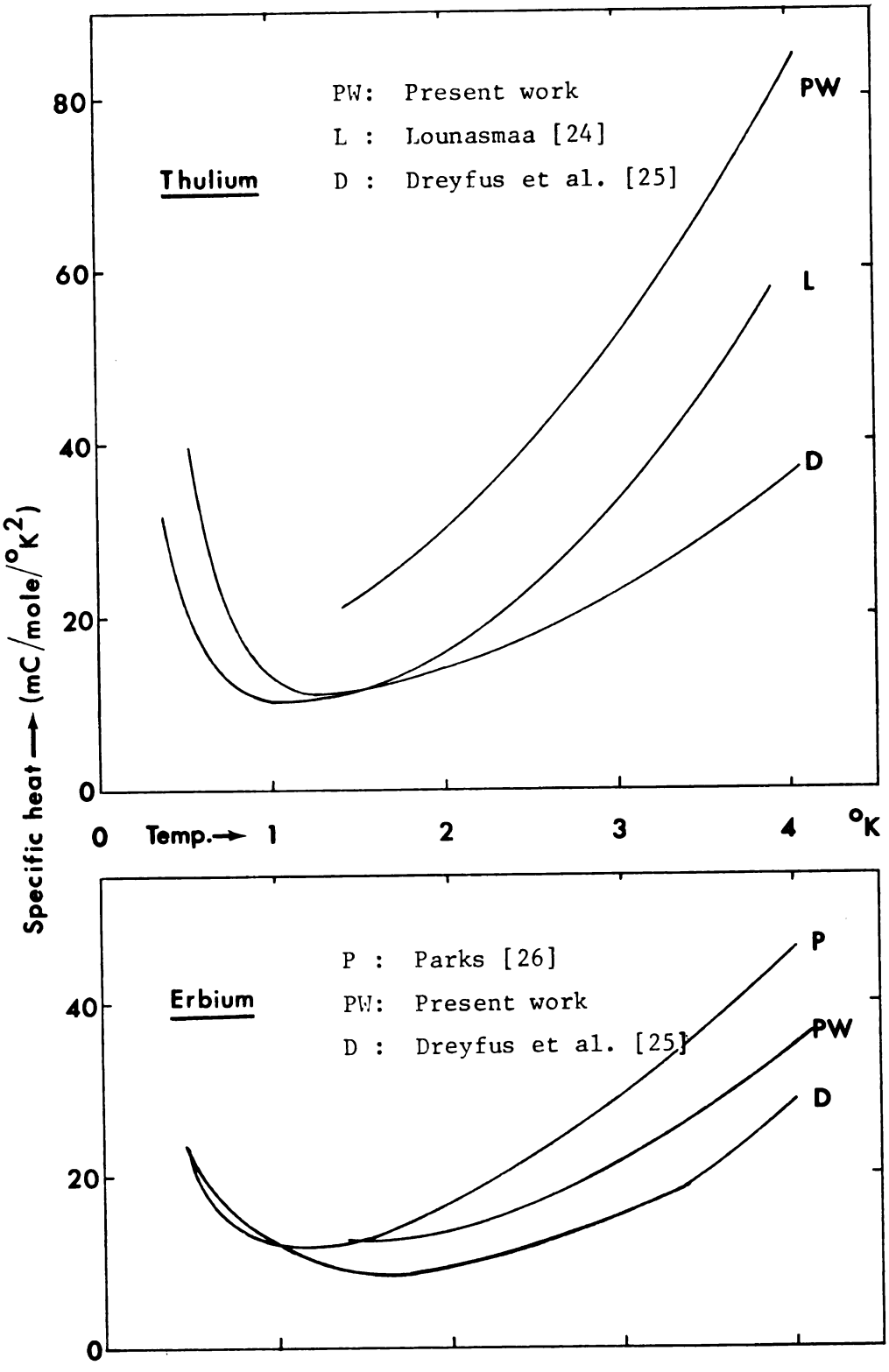

FIG. 20 Comparison of specific-heat data of different workers

As discussed in Chapter I, the current theories of the rare-earth metals are based on the localized 4f-band model. The 4f electrons are assumed to form partially filled bands and yet they do not contribute to the Fermi surfaces in the rare-earth metals. Only the three valence electrons form the conduction band, and hence a constant electronic specific heat is predicted for all the hcp lanthanides. The present results can not be explained by such a model.

If the localized 4f-band model were valid, the 5d band of the rare earths should be the major contributor to the Fermi surfaces in these metals, and to their electronic specific heats. According to the APW-calculations by Dimmock et al. [14-18] using such a model, the 5d band has a width of 6.8 eV as shown in Fig. 1. One may compare this with the 3d band in the first long period transition metals. Belding [52] calculated the 3d band in bcc paramagnetic Cr by using the tight-binding approximation, and obtained a comparable band width of about 5 eV. A close resemblance can be noted between this calculated result and the experimentally determined 3d energy band of Beck and co-workers [28] as shown in Fig. 21. Based on this

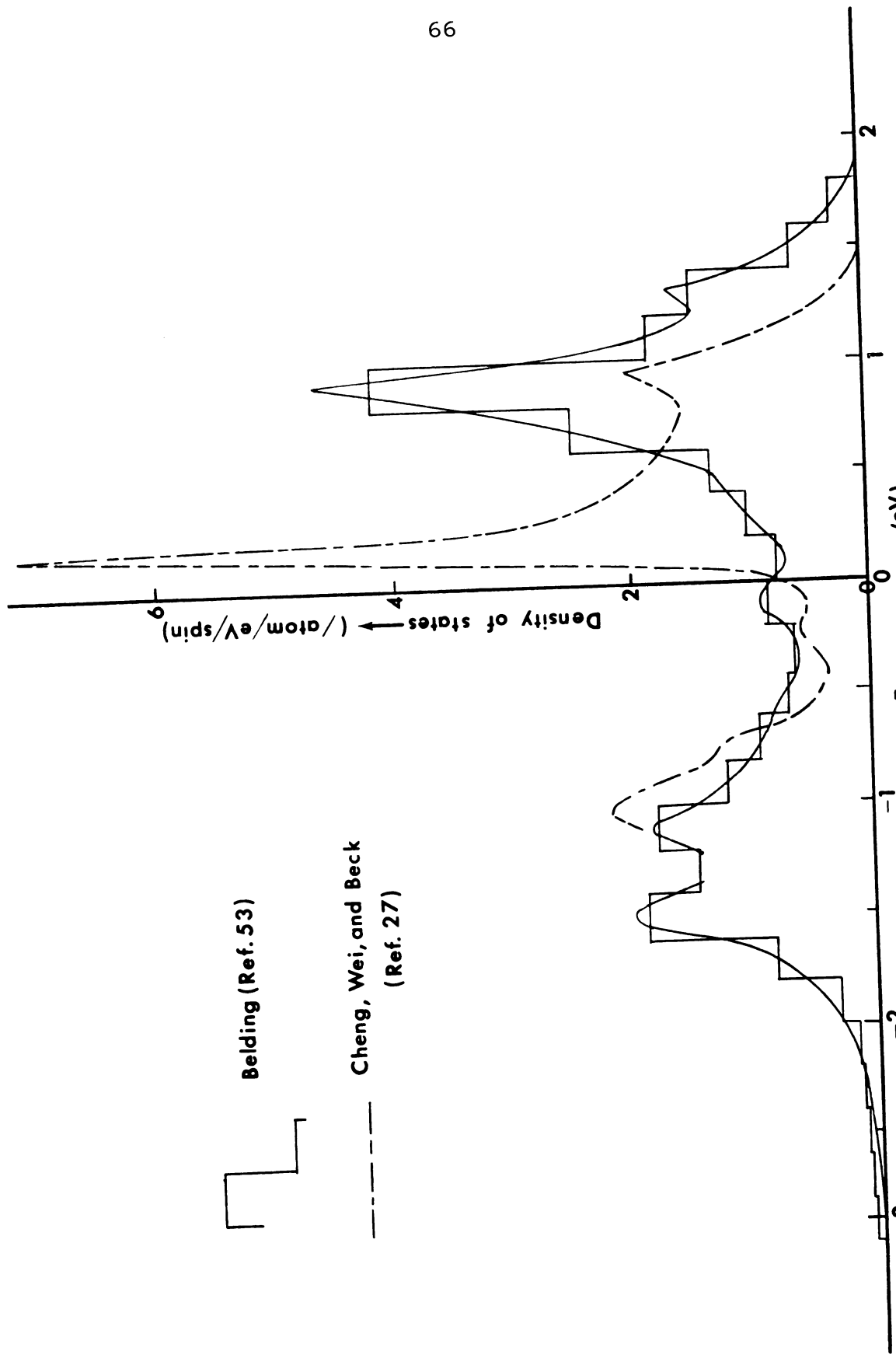

FIG. 21 Calculated and measured 3d-energy bands

evi

mod

the

tic

in

pe

re

th

dic

ha

mo

no

ne

3d

ti

th

sp

Th

to

an

tu

evidence Mott [29] corrected his earlier localized 3d-band model [27] for the transition metals. The calculated and the experimentally obtained 3d bands for the bcc transition metals do not differ to any appreciable extent except in the Cr-Fe alloy system. On the other hand, all the experimental evidence from the present work as well as the results of Lounasmaa [24] and Dreyfus et al. [25] indicate that the γ values are much larger than what might be predicted by the localized 4f-band model.

All the heavy rare-earth metals, except Lu which has a filled 4f band, are known to have a net magnetic moment at low temperatures. A localized 4f-band model is not necessarily needed to explain the low-temperature magnetic structures in these metals any more than a localized 3d-band model is required to explain the magnetic properties of the transition metals. Instead, it is possible that a narrow 4f band could split into up-spin and down-spin half-bands, which may or may not overlap as a group. The relative positions of the two half-bands with respect to the Fermi surface may vary from one rare-earth metal to another depending upon such factors as the crystal structure, the number of 4f electrons per atom and the exchange

interaction between the electrons. One may modify Mott's one-electron band model [23] so that each half-band, not necessarily localized, is built of seven overlapping one-electron bands. The density of states of each of these half-bands may contain peaks and valleys. When there is an integral number of 4f electrons in the metal, the Fermi surface is most likely to be near a valley. Such a model would explain the nearly uniform electronic specific-heat coefficients of the pure rare-earth metals as well as the large variations in the γ values of the alloys as those that are observed in the present work. A schematic diagram of such a proposed itinerant 4f-band model is shown in Fig. 22.

Additional work such as the room-temperature specific-heat measurements of alloys of the rare earths may help to confirm the proposed model. Should this itinerant 4f-band model be established, then it would not be necessary to resort to using the electron-phonon type enhancements in explaining the discrepancies between the theoretically predicted and the experimentally obtained electronic specific heats of the rare-earth lanthanides.

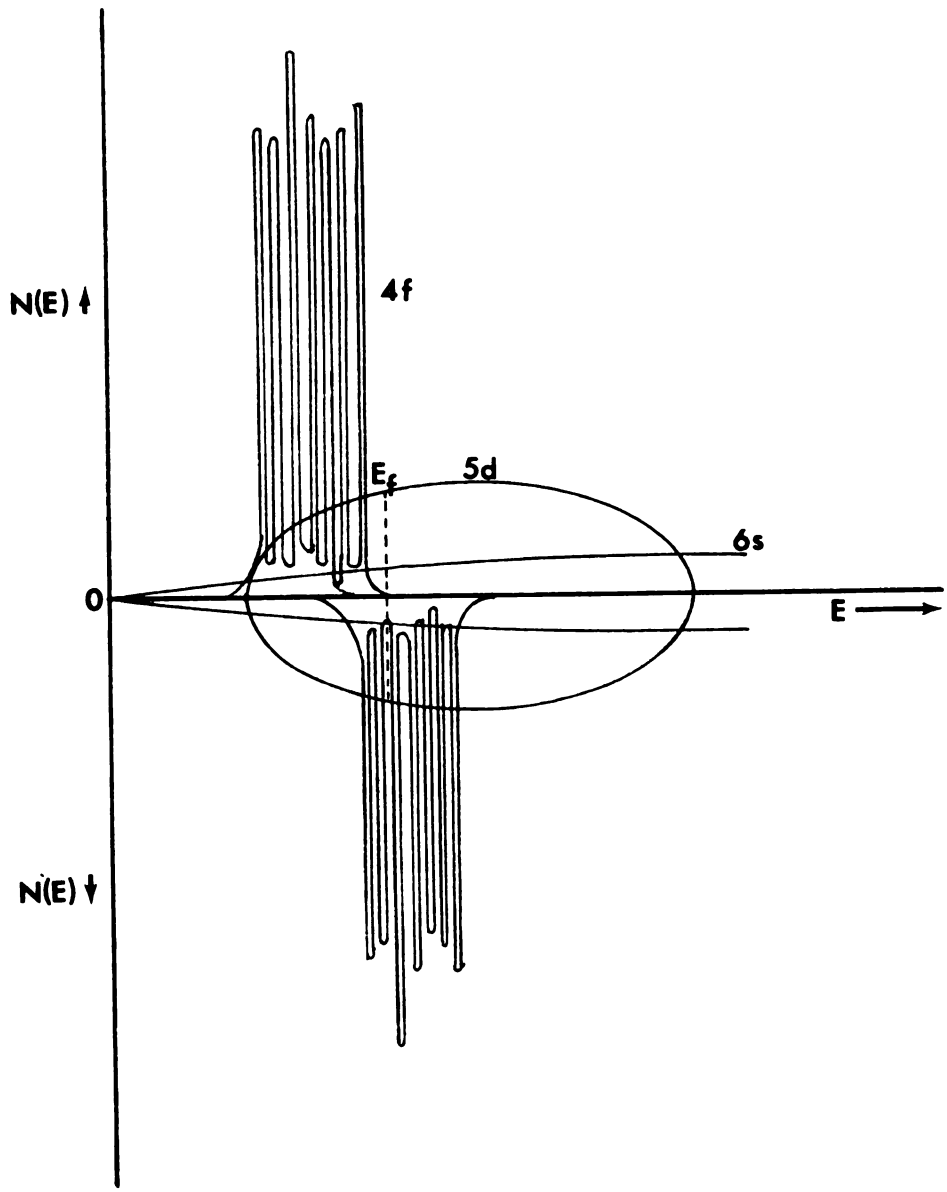

FIG. 22 Schematic itinerant 4f−band model

CHAPTER V

CONCLUSIONS

1. The specific heats of hexagonal close-packed Er and Tm metals and three isostructural Er-Tm alloys were determined in the temperature range of 1.3 to 4.2°K.

2. Barring possible complications due to the uncertainties in the magnetic properties of these samples and the effects of impurities, the electronic specific-heat coefficients obtained from the analyses of the specific-heat data range in values from 2.5 to 23.3 milli-cals/mole/$°K^2$. These values are two to some twenty times the constant value that might be predicted by a localized 4f-band model. Such discrepancies are too high to be accounted for by the electron-phonon and electron-magnon enhancements.

3. It appears possible that the 4f electrons in the rare-earth lanthanides may form energy bands which do contribute to the Fermi surfaces and hence to the specific

heats in the usual sense, and that they are better described as itinerant rather than localized.

4. Such an itinerant 4f-band model would explain the high electronic specific heats of the rare-earth metals and alloys. It may not introduce any more difficulties in explaining their complicated magnetic properties than the itinerant 3d-band model might have in the case of the transition metals.

1.

2.

3.

4.

5.

6.

7.

8.

9.

10.

11.

CHAPTER VI

REFERENCES

1. R. Marrus, W. A. Nierenberg, and J. Winocur, U.C.R.L. 9207, May 1960; also quoted by B. B. Cunningham, Rare Earth Research, III (127), Macmillan Co., N.Y., 1961.

2. F. H. Spedding, S. Legvold, A. H. Daane, and L. D. Jennings, Prog. Low Temp. Phys., II, Ch. 12, Ed.: C. J. Gorter, North Holland Pub. Co., Amsterdam, 1957.

3. T. Kasuya, Prog. Theor. Phys. (Kyoto), 16 (38), 1956,
   Ibid., ... 16 (45), 1956,
   Ibid., ... 22 (227), 1959.

4. K. Yosida and A. Watabe, Prog. Theor. Phys. (Kyoto), 28 (361), 1962.

5. R. J. Elliott and F. A. Wedgewood, Proc. Phys. Soc. (London), 81 (846), 1963.

6. J. O. Dimmock and A. J. Freeman, Phys. Rev. Letters, 13, #25 (199), 1964.

7. A. J. Freeman, J. O. Dimmock and R. E. Watson, Phys. Rev. Letters, 16, #3 (94), 1966.

8. R. E. Watson, A. J. Freeman, and J. O. Dimmock, Phys. Rev., 167, #2 (497), 1968.

9. D. J. Kim, Phys. Rev., 167, #2 (545), 1968.

10. O. K. Andersen and T. L. Loucks, Phys. Rev., 167, #2 (551), 1968.

11. A. Berman, M. W. Zemansky, and H. A. Boorse, Phys. Rev., 109, #1 (70), 1958.

12. L. D. Jennings, R. E. Miller, and F. H. Spedding, J. Chem. Phys., 33 (1849), 1960.

13. O. V. Lounasmaa, Phys. Rev., 129 (2460), 1963 (:Gd,Yb).

14. W. C. Koehler, H. R. Child, E. O. Wollan, and J. C. Cable, J. Appl. Phys., S32 (48), 1961.
Ibid., . . . S34 (1335), 1963.

15. W. C. Koehler, Phys. Rev., 126 (1672), 1962.

16. T. Kasuya, Megnetism, IIB (215), Ed.: Rado and Suhl, Acad. Press, N.Y., 1966.

17. H. Nigh, S. Legvold, and F. H. Spedding, Phys. Rev., 132 (1092), 1963.

18. P. M. Hall, S. Legvold, and F. H. Spedding, Phys. Rev., 109 (971), 1958.

19. R. V. Colvin, S. Legvold, and F. H. Spedding, Phys. Rev., 120 (741), 1960.

20. D. E. Hegland, S. Legvold, and F. H. Spedding, Phys. Rev., 131 (158), 1963.

21. C. Herring, Magnetism, IV, Acad. Press, N.Y., 1966.

22. K. A. Gschneidner Jr., Rare Earth Research, III (153), Ed.: LeRoy Eyring, Gordon and Breach Inc., N.Y., 1965.

23. N. F. Mott, Phil. Mag., 6 (306), 1961.

24. O. V. Lounasmaa,
Phys. Rev., 128, #3 (1136), 1962 (:Ho),
Ibid. ... 129, #6 (2460), 1963 (:Gd,Yb; same as 13),
Ibid. ... 133, #1A (211), 1964 (:Pr,Nd),
Ibid. ... 133, #1A (219), 1964 (:Lu)
Ibid. ... 133, #2A (502), 1964 (:Ce,Eu),
Ibid. ... 134, #6A (1620), 1964 (Tm)
Rare Earth Research, II (221), Ed.: Vorres, Gordon & Breach, Inc., N.Y., 1964 (Ce,Pr,Nd,Eu,Lu).

25. B. Dreyfus, B. B. Cunningham, A. Lacaze, and G. Trolliet, Compte Rendu, Acad. des Sciences (1764), 1961.

26. R. D. Parks, Rare Earth Research (225), Ed.: Nachman, and Lundin, Gordon & Breach, N.Y., 1962.

27. N. F. Mott and K. W. H. Stevens, Phil. Mag., 2 (1364), 1957.

28. C. H. Cheng, C. T. Wei, and P. A. Beck, Phys. Rev., 120 (246), 1960.

29. N. F. Mott, Adv. Phys., 13 (325), 1964.

30. B. Dreyfus, J. C. Michel, and A. Combiende, Proc. IX Intl. Conf. Low Temp. Phys. (1054), Plenum Press, N.Y., 1965.

31. A. Sommerfeld, Ann. d. Physiks, 28 (1), 1937.

32. E. C. Stoner, Proc. Roy. Soc. (London), A154 (656), 1936.

33. P. J. Tsang, Ph.D. Thesis, Mich. State Univ., 1968.

34. C. Kittel, Introduction to Solid State Physics, J. Wiley & Sons, N.Y., 1967.

35. F. Bloch, Z. Physik, 52 (555), 1928.

36. J. V. Kronendonk and J. H. van Vleck, Rev. Mod. Phys., 30, #1 (1), 1958.

37. D. T. Edmonds and R. G. Petersen, Phys. Rev. Letters, 2 (499), 1959.

38. E. S. R. Gopal, Specific Heats at Low Temperatures, Plenum Press, N.Y., 1966.

39. W. Marshall, Phys. Rev., 110 (1280), 1958.

40. B. Bleaney, J. Appl. Phys., 34, #2 (Part 2), (1024), 1963.

41. J. Mackowiak, Physical Chemistry for Metallurgists (160), Am. Elsevier Pub. Co., N.Y., 1966.

42. D. H. Dennison, M. J. Tschetter, and K. A. Gschneidner, J. Less-Common Metals, 10 (108), 1966,
Ibid. ... 11 (423), 1966.

43. C. T. Wei, Ph.D. Thesis, Univ. of Illinois, 1959.

44. W. R. Roach, J. C. Wheatley, and A. C. Mota de Victoria, Rev. Scientific Intr., 35, #5 (634), 1964.

45. N. B. S. Monograph 10, The 1958 He^4 Scale of Temperatures, H. van Dijk, M. Durieux, J. R. Clement, and J. K. Logan, 1960.

46. P. H. Keesom and N. Pearlman, Encyclopedia of Phys., Ed.: S. Fluge, 14 (297), 1956.

47. L. L. Isaacs and T. B. Massalski, Phys. Rev., 138, #1A (134), 1965.

48. R. M. Bozorth and R. J. Gambino, Phys. Rev., 147, #2 (487), 1966.

49. O. V. Lounasmaa and L. J. Sundstrom, Phys. Rev., 150, #2 (399), 1966.

50. T. A. Kaplan, Phys. Rev., 124 (329), 1961.

51. L. T. Crane, J. Chem. Phys., 36, #1 (10), 1962.

52. E. I. Belding, Phil. Mag., 4 (1145), 1959.

APPENDIX A

SWITCH SETTINGS FOR VARIOUS FUNCTIONS OF THE MEASURING DEVICES

Function	Settings of the switch										
	1	2	3	4	5	6	7	9	10	11	12
Standardization of Potentiometer	-	C	C	D	D	-	-	-	ON	U	ON
Standardization of Heating current	ON	D	C	U	U	-	-	-	ON	U	OFF
Standardization of Measuring current	-	U	C	U	U	-	adj	ON	ON	U	OFF
Measuring Heater EMF	ON	C	D	D	D	-	-	-	ON	U	OFF
Measuring Thermometer EMF	-	C	U	D	D	2	adj	ON	ON	U	OFF
Calibration of DC Amplifier and Rec.	-	C	U	D	D	3	-	ON	OFF	D	OFF
Recording Thermometer Resistance	**	C	U	D	D	4	adj	ON	OFF	D	OFF

**On for heating, Off for stand-by.
#8 Switch is ON all the time.
C = Center; U = Up; D = Down; adj = Adjust.

APPENDIX B

EXPERIMENTAL PROCEDURE

Considering the time at which liquid helium is transferred from the container to the cryostat as the zero-hour, the experimental procedures are listed below:

-48:00 Weigh the two sample halves. Prepare the specimen: Sandwich the sample-halves with the heater-thermometer assembly. Weigh the specimen and suspend it in the calorimeter. Solder the leads to the four kovar-seal connector-pins. Check the electrical system for open- and short-circuits by measuring the heater and the thermometer resistances. Solder the colorimeter can in position. Load the calorimeter system into the inner dewar. Position the cathetometer and adjust its levels. Turn on the main-switch MS1 (see figure 7) for the electrical system to stabilize. Evacuate the calorimeter and start the diffusion pump.

Appendix B (cont.)

-42:00 Repair any leaks in the calorimeter system if necessary till a stable reading is obtained on the cold-cathode vacuum gage in the lower range of 10^{-5} torr. without the cold-trap.

-16:00 Turn off the diffusion pump. Prepare the dewar system for liquid-nitrogen transfer: Evacuate the middle jacket of the liquid-helium dewar, and flush it with dry nitrogen gas. Close valve 6 (figure 5) when the nitrogen inside the middle-jacket is at 200 microns. Evacuate the inner-dewar slowly by opening valves V1, V2, V3, and flush it three times with helium gas. Release the system to helium gas and maintain ¼-psig pressure. Flush and evacuate the calorimeter system with the helium gas three times and close the valve CV (figure 4), leaving the helium gas inside at 700 microns pressure. Transfer liquid nitrogen into the outer dewar.

-4:00 Standardize the potentiometer, and adjust the decade-resistors R14, R16 to set the heater and

Appendix B (cont.)

the thermometer currents at 0.1mA and 1.0μA respectively. Measure the thermometer and the heater resistances at the liquid-nitrogen temperature in order to check the electrical system. (See Appendix A.) Evacuate the calorimeter, and start the diffusion pump. (The end-vacuum should be in the lower range of 10^{-6} torr. with the cold-trap; if not, lower the outer-dewar to let the system warm up to room temperature, and go back to -42:00.) Refill the outer-dewar with liquid nitrogen.

-1:00 Evacuate the liquid-helium transfer-tube jacket. Position the liquid-helium container on a fork-lift, flush the transfer-tube with helium gas and insert it in the container. Check the pressure of the helium gas in the inner-dewar for ¼-psig. Remove the inlet screw IS and insert the delivery end of the transfer-tube into the inner-dewar.

0:00 Supply helium gas to the liquid-helium container at 2/3-psig to start the liquid-helium transfer.

Appendix B (cont.)

(Stop the transfer immediately if the calorimeter vacuum deteriorates, or if the liquid-helium level begins to fall at any time. Go back to -42:00 in the former case, and start at -1.00 if a fresh liquid-helium container is available in the latter case.) Open valve MV1 (figure 6), start pump P3, and open valve P3V slowly. Turn off the diffusion pump, open valve CV to release helium gas into the calorimeter, and close valves CV and P2V to arrest about 400 microns of helium gas in the calorimeter. Collect the liquid helium up to 4" below the top of the inner-dewar. (The transfer usually takes about 10 mins.) Open the safety valve SV (figure 5), and retain it in that position. Remove the transfer tube, re-instate and tighten the inlet screw IS.

0:30 Standardize the potentiometer again. Set and note the decade-resistor R14 readings for 0.05, 0.07, 0.1, 0.2, 0.3, 0.4, 0.5, 0.7, and 1.0 milliamperes of current through the heater.

Appendix B (cont.)

Measure the heater resistance. Set the decade resistor R16 to get 1.0μA thermometer current. Measure the thermometer resistance. (Always maintain the sum of the last two readings constant by compensating the R16 reading when measuring the thermometer resistance.) Check the recorder calibration with the potentiometer.

1:00 Start calibration: Measure the level of the liquid-helium bath. Close valve MV1. Note the potentiometer reading. Take the mercury-manometer readings and the Stokes-gage reading. Start pump P1. Drop safety-valve Sv, and simultaneously but slowly open the needle-valve V1 (figure 4) to pump the liquid-helium vapor at a slow rate. Balance most of the voltage-drop across the thermometer with the EMF from the potentiometer. As the unbalanced voltage-drop reading fed to the recorder slowly decreases and passes the zero of the recorder scale at the 50μV-scale of the DC-amplifier close the valve MV1 to the manometer. Note the liquid-helium head, the potentiometer, manometer,

Appendix B (cont.)

and the Stokes'-gage readings. Open MV1 slowly, set the potentiometer reading at the next desired value, and open valves V1, V2, and V3 slowly as required. Compensate R14 for the thermometer-resistance, and take readings as described. Repeat the procedure to collect about ten sets of data above the lambda-point at increasing gaps of potentiometer-readings. (Below the λ-point of liquid helium the hydro-static correction need not be noted.) Switch over to the oil-manometer at below 40 torr., and to the McLeod-gage at about 5-torr. liquid-helium vapor-pressure.

7:00 Reset the heater current at 0.1mA, and measure the heater resistance at the lowest temperature attained. Turn off the heater and the thermometer currents, the high-sensitivity galvanometer key of the potentiometer, and turn on the shunt switch S10 (Fig. 7). Start pump P2, open valve P2V, and turn on the diffusion pump to remove the exchange-gas in the calorimeter. Set the decade-resistor

R14 corresponding to the heater current of 0.07mA. Turn off the shunt switch S10 and balance most of the voltage-drop across the thermometer with the potentiometer EMF so that the recorder pointer stays close to the zero on the 200μV scale. Start the recorder-chart, set the counter-reading to zero, and turn on the heater-current. Quickly compensate R16 for the anticipated change in the thermometer resistance, and turn off the heater-current when the recorder pointer approaches the extreme of the recorder-scale. Take 25 to 40 readings in the 1.3° to 4.2°K temperature range at decreasing potentiometer-reading gaps, increase the heater current and decrease the recorder scale so that the heating curves extend to the full scale of the recorder in about 10 to 60 seconds time.

APPENDIX C

COMPUTER PROGRAMS

```
        PROGRAM REMPLOT
       DIMENSION R(40), P(40), T(80), PI(80), X(40), Y(40), CV2(80),
      1 RI(80), R2(80), T1(80), T2(80), TM(80), CIH(80), RST(80),
      1 TT(80), C(10), TSQ(80), RR(2,80), IC(80), PR(80), SR1(80),
      1 SR2(80), LBL(15), NPC(4), PRM(4,3), XH(101,4), YV(101,4), LB(15,10),
      1  XSQ(80), YSQ(80), EXPTYPE(10), P1(40), P2(40), DT(40), DT1(80),
      1 RSTC(80), ERPCT(80), A(10,10), B(10), TC(40), CVM(80), CVN(80),
      6  CVMN(80), CVMNC(80), CVEA(80), CVEAC(80), IB(80), TX(40), CV1(80),
      7  CVLAT(80), CVEM(80), CVEMT(80), CVMAG(80)
        TYPE REAL LAMBDA
        COMMON/XS/XL/YS/YL
C       SQRTF(LOGF(R)/(T*2,3026))=C(1)+C(2)*LOGF(R)/2.3026+
C      1     C(3)*(LOGF(R)/2.3026)**2
  100    FORMAT (8I10)
 1000   FORMAT (1H1)
 1001   FORMAT (10A8)
 1010   FORMAT (3A8)
  200   FORMAT (8F10.7)
  201    FORMAT (/8X, 2F15.3, 3F15.7, F14.3, F16.7, I5/)
  202   FORMAT(18X,*R*,14X*P*,14X*T*,14X*X*,14X,*Y*,11X,*PCT.ERROR*,
      1 6X,*DEL,T*,4X,*D-NO.*/)
 2029   FORMAT (14X,*A*,20X,*B*)
  203   FORMAT (14X,*A*,20X,*B*,20X,*C*)
  300   FORMAT(//6F20.10//)
  301   FORMAT (8X,3F10.3,F9.4,5F12.7,E16.3,15/)
  302   FORMAT(12X,*R1*,8X,*R2*,8X,*TM*,8X,*CIH*,9X,*T*,9X,*CV2*,9X,*TSQ*,
      1  9X,*CV/T*,6X,*CV/T-CALC.*,6X,*PCT.ERROR*,4X,*C-NO*,/)
```

```
 303  FORMAT(/12X,*GAMMA*,14X,*ALPHA*,14X,*THETA*)
 304  FORMAT (/,14X,*FN1*,15X,*FN2*,15X,*FRH*,15X,*ZE*,19X,*CFRH*,
     1   18X,*CFCIH*)
3030  FORMAT (/12X,*GAMMA*,14X,*ALPHA*,12X,*MAG,TERM(S)*,12X,*NUCLEAR*,
     1* CONTRIBUTION TO SP,HEATS=(T)PR-3,-4,-5 TERMS*,/)
3040  FORMAT (/14X,*FN1*,15X,*FN2*,15X,*FRH*,15X,*ZE*,19X,*CFRH*,
     1    15X,*CFCIH*, 9X,*CFTM*/)
 310  FORMAT(/12X,*GAMMA*,14X,*ALPHA*,14X,*BETA*,14X,*THETA*)
 320     FORMAT (/12X, *GAMMA*,10X,*BETAMAG*,14X,*ALPHALAT*,/)
 400  FORMAT  (2X,*PO-RD*,6X,*SM-R-1*,3X*T-RES-1*,3X,*SM-R-2*,3X,
     1 *T-RES-2*,5X,*C-NO*,4X,*TSQ*,8X,*CV(E+A)*,6X,*PCT.ERROR*,6X,
     2   *CV(M)*,6X,*CV(N)*/)
 404  FORMAT      (/5F10.3,15,2F12.7,E14.4,2F13.7,/)
 407  FORMAT  (3X,*NO.    DELTA T     TEMP.         SP.HT.      CV(E+M)
     1     NO.        T-SQ       CV/T       CV(E+M)/T     CV(LAT)    CV
     2(NUC)/T  NO.*/)
 408  FORMAT (15, 4F13.6, I8, 5F13.6, 15/)
  50  FORMAT (110, 6F10.4)
 500  FORMAT (30X,10A8,/)
 555  FORMAT (*0*10X* ZERO ERROR=* F7.3,*-OHMS*/)
 556     FORMAT (*0*10X* ASSUMED DEBYE TEMP=* F7.3/)
 600  FORMAT (8I10)
  65    FORMAT (I10, 5F10.5)
  69  FORMAT (*0*10X*I1=*,13,*M=*,13,*12=*,13,*J=*,13,*T=*,F5.3,*X=*,
     1  F7.3,*Y=*,F7.3,/)
7501  FORMAT (/30X,*MATRIX ELEMENTS*,/)
7502    FORMAT (*0*10*A(I,J)=*7E15.4,/)
 786  FORMAT (/ *0*10X*THETA=*, F7.3 /)
 787  FORMAT (7F17.10)
 788   FORMAT (*0*10*CMAG FROM ENTROPY CONSID. =* F17.10/)
  99  FORMAT (I10)
      READ 1010, (LB(MB,1), MB=4,13)
      READ 100, NCRV, LN, NCOPYS
      MLB=1
      DO 5 L=1,NCRV
      DO 5 MB=4,13
```

```
     5 LB(MB,L)=LB(MB,1)
C        CALIBRATION PROGRAM BEGINS =
    10 READ 100, M1, N, M2
         IF ( EOP,60) 20, 25
    20  CALL PLOT (20.,0.,-1)    $     GO TO 2000
    25 READ 1001, (LB(MB,1), MB=1,3)
          READ 1001, EXPTYPE
       READ 200, ZE
   262 I-1=1  $  12=1  $  M=M1
    26   DO 27 I=I1,M
    27   READ 50, IC(I), R(I), P(I), P1(I), P2(I), T1(I), T2(I)
       READ 200, ZE,CNUC1,CNUC2,CNUC3
         READ 100, MD, N, K1, K2, K3, K4, K5
         READ 200, FN1, FN2, FRH,  CFRH, CFCIH, DTEMP
         DO 60  I=1,MD
    60   READ 65, IB(I), PR(I), CIH(I), TM(I), SR1(I), SR2(I)
       DO 30 I=I1,M
        TX(I)=T1(I)+(T2(I)-T1(I))/(P2(I)-P1(I))*(P(I)-P1(I))
    30   TT(I)=1.0
       PRINT 1000
       PRINT 500, (LB(MB,1), MB=1,3)
          PRINT 500, EXPTYPE
          PRINT 555, ZE
       PRINT 202
        J=M
        CMAG=0.      $    CFTM=0.
       IF (M2) 312, 312, 311
   311    M=M2  $  LAMBDA=2.172   $   JX=1 $  J=M12
   312  DO 35 I=I1,M
       R(I)=R(I)-ZE
       X(I)=LOGF(R(I))/2.302585
    35 Y(I)=SQRTF(X(I)/TX(I))
       CALL MCPALS(J.N,0.,TT,X,Y,RR,C,IDEG)
       N2=N+2
       DO 40 I=N2,10
    40 C(I)=0.0
```

```
      DO 45 I=11,M $  TC(I)=X(I)/(C(1)+C(2)*X(1)+C(3)*(X(I)**2))**2
RR(2,I)=RR(2,I)*100
```

```
        DO 45 I=I1,M $  TC(I)=X(I)/(C(1)+C(2)*X(I)+C(3)*(X(I)**2))**2
       RR(2.I)=RR(2,I)*100.
 45    DT(I)= TX(I)-TC(I)
       PRINT 201,(R(I),P(I),TX(I),X(I),Y(I),RR(2,I),DT(I),IC(I), I=I1,M)
       K=N+k   $           L=3
       IF (C(L)) 2031,2030,2031
 2030  PRINT 2029
       GO TO 2032
 2031  PRINT 203
 2032  PRINT 300, (C(I), I=1,K)
C      CALIBRATION PROGRAM ENDS= REGULAR MAIN PROGRAM FOLLOWS
       PRINT 1000
       PRINT 500, (LB(MB,1), MB=1,3)
          PRINT 500, EXTYPE
       FJ=4.184
       FRH=FRH*CFRH
          DO 70 I=12,MD
       CIH(I)=CFCIH*CIH(I)
       R1(I)=PR(I)-SR1(I)-ZE
       R2(I)=PR(I)-SR2(I)-ZE
       X=LOGF(R1(I))/2.302585
       Y=LOGF(R2(I))/2.302585
       T1(I)=X/(C(1)+C(2)*X+C(3)*(X**2))**2
       T2(I)=Y/(C(1)+C(2)*Y+C(3)*Y**2))**2
       T(I)=0.5*(T1(I)+T2(I))
        DT1(I)=T](I)-T1(I)
       TSQ(I)=T(I)*T(I)
       CVI(I)=(0.698+0.0485*TSQ(I))/4184.   $  CVT=CV1(I)
C      RST(I)=C(1)+C(2)*T(I)**2+C(3)*T(I)**0.5+C(4)*T(I)**1.5+
C     1            C(5)*(T(I)**(-3)) +C(6)*(T(I)**(-4)) +C(7)*T(I)**(-5)
        RST(I)=(CIH(I)/1000.)**2*FRH*TM(I)/(FN2*DT1(I)* T(I)*FJ)-FN1*CVT/
      1 FN2
       CV2(I)=RST(I)*T(I)   $  IF (M2) 70, 70, 67
    67 IF (JX-2) 671, 70, 70
   671   IF (T(I)-LAMBDA) 68, 68, 70
   68  I1=M2+1  $  M-M1  $  I2=I+1  $  J=M1=M2  $  JX=JX=+1
       PRINT 69, I1,M,I2, J, T(I), X, Y
```

```
      GO TO 312
70    CONTINUE          $          M=MD
```

```
      GO TO 312
 70     CONTINUE    $     M=MD
 71    DO 73  I=1,7  $  B(I)=0.0  $  C(I)=0.8
 72    DO 73  J=1,7
 73    A(I,J)=0.0  $     A(1,1)=M
     DO 75 I=1,M  $  SQT=SQRTF(T(I)) $ T3=TSQ(I)*T(I) $ T15=T(I)*SQT
      T25=TSQ(I)*SQT  $  T35=T3*SQT  $  T4=TSQ(I)*TSQ(I)  $  T45=T4*SQT
      T5=T4*T(I)  $  T6=T3*T3  $  T7=T4*T3  $  T8=T4*T4  $  T9=T5*T4
      T10=T5*T5
      A(1,2)=A(1,2)+TSQ(I)  $  A(1,3)=A(1,3)+SQT  $  A(1,4)=A(1,4)+T15
      A(1,5)=A(1,5)+1./T3  $  A(1.6)=A(1.6)+1./T4  $  A(1.7)=A(1.7)+
    1                                                          1./T5
 732  A(2,2)=A(2,2)+T4  $  A(2,3)=A(2,3)+T25  $  A(2,4)+A(2,4)+T35
      A(2,5)=A(2,5)+1./T(I)  $  A(2,6)=A(2,6)+1./TSQ(I)
           A(2,7)=A(2,7)+1./T3
      A(3,3)=A(3,3)+T(I)  $  A(3,5)=A(3,5)+1./T25  $  A(3,6)=A(3,6)+
    1          1./T35  $  A(3,7)+A(3,7)+1./T45
      A(4,4)=A(4,4)+T3  $  A(4,5)=A(4,5)+1./T15
      A(5,5)=A(5,5)+1./T6  $  A(5,6)=A(5,6)+1./T7
                          A(5,7)=A(5,7)+1./T8
      A(6,7)=A(6,7)+1./T9           $         A(7,7)=A(7,7)+1./T10
 736  B(1)=B(1)+RST(I)  $  B(2)=B(2)+RST(I)*TSQ(I)
      B(3)=B(3)+RST(I)*SQT  $  B(4)=B(4)+RST(I) *T15
      B(5)=B(5)+RST(I)/T3  $  B(6)+RST(I)/T4
      B(7)=B(7)+RST(I)/T5
      CONTINUE  $  A(1,1)=M  $  A(3,4)=A(1,2)  $  A(4,6=A(3,5)
       A(4,7)=A(3,6)  $  A(6,6)=A(5,7)
      DO 125 I=2,7  $  J1=I-1  $      DO 125 J=1,J1
 125  A(I,J)=A(J,I)
         PRINT 7501
      DO 7503  I=1,7
      PRINT 7502,(A(I,J), J=1,7)
7503   CONTINUE
      ID=7  $  IF(K5  .EQ.  0)  ID=6
76    IF (K4)  761,761,764
761   DQ 762  I=1,7
 762  A(6,I)=A(7,I)          $       DO 763  I=1,7
```

```
 763   A(I,6)=A(I,7)  $  ID=ID-1 $  B(6)=B(7)
 764   CONTINUE
 77    IF (K3)  771,771,774
 771   DO 772  I=1,7   $   A(I,5)=A(I,6)
 772   A(I,6)=A(I,7)       $   DO 773  I=1,7   $   A(5,1)=A(6,I)
 773  A(6,I)=A(7,I)  $  ID=ID-1  $  B(5)-B(6)  $  B(6)=B(7)
 774   CONTINUE
 78    IF (K2)  781,781,784
 781   DO 782 I=1,7  $  A(I,4)=A(I,5)  $  A(I,5)=A(I,6)
 782  A(I,6)=A(I,7)  $  DO 783  I=1,7  $  A(4,I)=A(5,I)  $  A(5,I)=A(6,I)
 783  A(6,I)=A(7,I)  $  ID=ID-1  $  B(4)=B(5)  $  B(5)=B(6)  $  B(6)=B(7)
 784   CONTINUE
       IF (K1)  7841,7841,7844
7841   DO 7842 I=1,7  $  A(I,3)=A(I,4)  $  A(I,4)=A(I,5)  $  A(I,5)=A(I,6)
7842   A(I,6)=A(I,7)  $  DO 7843  I=1,7  $  A(3,I)=A(4,I)
                                            A(4,I)=A(5,I)  $  A(5,I)=A(6,I)
7843  A(6,I)=A(7,I)  &  ID=ID-1  $  B(3)=B(4)  $  B(4)=B(5)  $  B(6)=B(7)
7844   CONTINUE
        PRINT 7501
        DO 785 I=1,ID  $   PRINT 7502,  (A(I,J), J=1, ID)
785    CONTINUE
      PRINT 1000
      PRINT 500, (LB(MB,1), MB=1,3)
         CALL GAUSS (ID,A,B,C)
79     IF (K1)  791,791,792
791    C(7)=C(6)  $  C(6)=C(5)  $   C(5)=C(4)  $   C(4)=C(3)  $  C(3)=0.0
792    CONTINUE
793    IF (K2) 794,794,795
794    C(7)=C(6)  $  C(6)=C(5)  $  C(5)=C(4)  $  C(4)=0.0
795    CONTINUE
       IF (K3)  796,796,797
796    C(7)=C(6)  $  C(6)=C(5)  $  C(5)=0.0
797    CONTINUE
       IF (K4)  798,798,799
798    C(7)=C(6)  $  C(6)=0.0
799    CONTINUE
       THETA= (465.00788718/(C(2)))**0.33333
```

```
        DO 80, I=1,M $  CVM(I)=C(3)*T(I)**0.5+C(4)*T(1)**1.5
       CVN(I)=C(5)/T(I)**3+C(6)/T(I)**4+C(7)/T(I)**5
       CVMNC(I)=CVM(I)+CVN(I)
       CVEAC(I)=C(1)+C(2)*T(I)**2 $  RSTC(I)=CVEAC(I)+CVMNC(I)
       ERPCT(I)=((RST(I)-RSTC(I))/RSTC(I))*100.0
       CVEA(I)=RST(I)-CVMC(I)
       XH(I,1)=TSQ(I)  $  YV(I,1)=CVEA(I)*1000.0
  80   CONTINUE
       PRINT 555, ZE
        PRINT 302
       PRINT 301, (R1(I),R2(I),TM(I),CIH(I),T(I),CV2(I),TSQ(I),
     1  RST(I), RSTC(I), ERPCT(I), IB(I), I=1,M)
       PRINT 3030
      PRINT 787, (C(I), I=1,7)
       PRINT  788, CMAG
      PRINT 786, THETA
      CALL MCPALS(M,N,0.,TT,TSQ,CVEA,RR,C,IDEG)
      PRINT 3040
      PRINT 787, FN1,FN2,FRH,ZE,CERH,CFCIH,CFTM
      K=N-1  $   IF (K) 3031, 3030, 3031
3030  PRINT 303
      GO TO 3032
3031  PRINT 310
3032  PRINT 300, (C(I), I=1,K), THETA  $     SX=0.0  $  SL=20.0
        NPC(1)=M $ NCG=1 $ LSQDEG=N $ MNPC=101 $ YS=0.0 $ YL=100.
      PRM(1,1)=C(1)*10.0**4 $ PRM(1,2)=C(2)*10.0**5  $  PRM(1,3)=THETA
      DO 9 I=1, NCOPYS
      NL=NL+1
      IF (NL.GT.MLB) NL=MLB
      DO 6 MB=1,13
    6 LBL(MB)=LB(MB,NL)
        NC=NCG
        CALL     GRAPH (YV,XH,NPC,PRM,LBL,MNPC,NCG,NCRV,LN,LSQDEG)
      CALL PLOT (300,X,3)
    9 CONTINUE
      PRINT 1000
      PRINT 500, (LB(MB,1), MB=1,3)
```

PRINT 304

```
      PRINT 304
      PRINT 300, FN1,FN2,FRH,ZE,CFRH,CFCIH
      PRINT 400
      PRINT 404, (PR(I),SR1(I),R1(I),SR2(I),R2(I),IB(I),XH(I),YV(I),
     1   RR(2,I), CVM(I), CVN(I), I=1,M)
      PRINT 786, THETA
        PRINT 1000  $  PRINT 500,  (LB(MB,1), MB=1,3)
        PRINT 500, EXPTYPE
       IF ( CNUC1. EQ. 0.)  CNUC1=C(5)  $  CNUC2=C(6)  $  CNUC3=C(7)
      DO 1500, I= 1,MD
       CVN(I)= CNUC1/(T(I)**3)  +  CNUC2/(T(I)**4)  +  CNUC3/(T(I)**5)
      CLATT= 465,00788718/(DTEMP**3)  $  CVLAT(I)= CLATT*(T(I)**2)
       CVEMT(I)=RST(I)-(CVN(I)+CVLAT(I))          $ CVEM(I)=CVEMT(I)*T(I)
 1500 CONTINUE
      PRINT 407  $  PRINT 408,(IB(I),DT1(I),T(I),CV2(I),CVEM(I),
     1 IB(I),TSQ(I),RST(I),CVEMT(I),CVLAT(I),CVN(I),IB(I),I=1,MD)
       C(2)=CLATT   $   THETA= (465.0078818/(C(2)))**0.33333
                      PRINT 787, (C(I), I=1,5), THETA
C      ANALYSIS OF ELECTRONIC AND MAGNETIC SPECIFIC-HEAT CONTRIBUTIONS
      N=1 $  CALL MCPALS(M,N,O.,TT,TSQ,CVEMT,RR,C,IDEG)
       PRINT 1520, C(1), C(2)
 1520 FORMAT(/*0*10X*ELECTRONIC SP-HEAT=*F10.7,10X,*MAGNETIC SP-HT=*F10.
     17/)
      PRINT 1000
      GO TO 10
C        ADD A DECK OF SUB-ROUTINES= GRAPH THRU GAUSS =IN BINERY DECK
 2000  CONTINUE
      END
```

APPENDIX C

PART II

SUBROUTINES

```
      SUBROUTINE GRAPH (YV,XH,NPC,PRM,LBL,MNPC,NCG,NCRV,LN,
                        LSQDEG,LP)
      DEMENSION YV(MNPC,NCG),XH(MNPC,NCG),NPC(4),PRM(4,3),
                LBL(15)
      COMMON/GRA/LSD
      DATA (NCURVE=0
      LSD=LSQDEG
C     INITIALIZATION
      CALL PLOT (0.,0.,0, 80., 80.)
      CALL PLOT (0.,-13.75,2)
      CALL PLOT (0.,0.,0)
      CALL PLOT (2.,3.,2)
      CALL PLOT (0.,0.,0)
      IUB=(NCRV/NCG)*20+20
      CALL PLOT (IUB,X,3)
C     GRID
      FN=NCH-1 $ YLBY = FN*0.25+11.0
      CALL CHAR (YLBT,0.0,LBL(1),8,0,0,.15,.1)
      CALL CHAR (YLBT,1.25,LBL(2),8,0.0.,15,.1)
      CALL CHAR (YLBT,2.50,LBL(3),8,0,0,.15,.1)
      CALL PLOT (0.,0.,2)
             FLN=10.0
      IF (LN.NE.0) FLN=0.1
```

```
      DO 2 I=2,10,2
      A=I-1
      CALL PLOT (0.0,A,2)
      CALL PLOT (FLN,A,1)
      CALL PLOT (FLN,A+1.,2)
      CALL PLOT (0.,A+1.,1)
    2 CONTINUE
      CALL PLOT (0.,0.,1)
      DO 3 I=2,10,2
      A=I-1
      CALL PLOT (A,0.0.2)
      CALL PLOT (A,FLN,1)
      CALL PLOT (A+1.,FLN,2)
      CALL PLOT (A+1.,0.,1)
    3 CONTINUE
      CALL PLOT (0.,0.,1)
      CALL PLOT (0.,0.,2)
C     SCALE X
      CALL CHAR (-1.0,2.00,LBL(4),8,0.0.,15,.0)
      CALL CHAR (-1.0,3.25,LBL(5),8,0.0,.15,.1)
      CALL CHAR (-1.0,4.50,LBL(6),8.0.0,.15.,1)
      XS=0.0
      XL=20.0
      C=(XL-XS)/10.0
      ENCODE (6,4,IS)XS
    4 FORMAT (F6.2)
      CALL CHAR (-0.25,-0.26,IS,6,0.0,1./8.,1./12.)
      B=XS
      DO 5 I=1,10
      FF=I  $  F=FF=0.26  $  G=B+C
      ENCODE (6.4,JS)G
      CALL CHAR (-0.25,F,JS,6,0.0,1./8.,1./12.)
      B=G
    5 CONTINUE
C     SCALE Y
      CALL CHAR (2.00,-1.5,LBL(7),8,90.,.15,.1)
      CALL CHAR (3.25,-1.5,LBL(8),8,90.,.15,.1)
      CALL CHAR (4.50,-1.5,LBL(9),8,90.,.15,.1)
      YL=20.0
      YS=0.0
      C=(YL-YS)/10.0
      ENCODE (8,7,KS)YS
    7 FORMAT (F8.3)
      CALL CHAR (0.0,-1.10,KS,8,0.0,1./8.,1./12.)
      B=YS
      DO 9 I=1,10
      F-1  $  G=B+C
      ENCODE (8,7,LS)G
      CALL CHAR (F,-1.10,LS,8,0.0,1./8.,1./12.)
      B=G
    9 CONTINUE
```

```
C       PARAMETER LIST
        DO 20 I=1,3
        YLB=FN*0.25+10.25  $  XLB=3*(I-1)  $  LL=I+9
        CALL CHAR (  YLB,XLB,LBL(LL),8,0.0,.15,.1)
        DO 20 NC=1, NCG
        FN1=NCG-NC  $  YP=FN1*0.25+10.25  $  XP=XLB+1.25
        IF (I.NE,3) GO TO 17
        NCURVE=NCURVE+1
        ENCODE (3,100.NCVE)NCURVE
  100   FORMAT (I3)
        CALL CHAR (YP,9.870,NCVE,3,0.,1./8.,1./12.)
        IF (NCG.EQ.1) GO TO 17
        YSY=YP+0.1  $  XSY=9.0
        CALL SYMBOL (NC,YSY,XSY,80.,80.)
   17   NCM1=NC-1
        IF (NC.GT.1.AND.PRM(NC,I).EQ.PRM(NCM1,I)) GO TO 20
        ENCODE (8,15,JP1)PRM(NC,I)
   15   FORMAT (F8.3)
        CALL CHAR (  YP,  XP,JP1,8,0.,.15,.1)
   20   CONTINUE
        CALL PLOT (0.,0.,2,80.,80.)
        CALL CURVE (YV,XH,NPC,MNPC,NCG,XL,XS,YL,YS,LP)
        CALL PLOT (0.,0.,0.80.,80.)
        CALL CHAR (12.5,0.,LBL(13),8,0.,0.5,1./3.)
        CALL PLOT (20.,0.,2)
        END


        SUBROUTINE CURVE (YV,XH,NPC,MNPC,NCG,XL,XS,YL,YS,LP)
        DIMENSION YV(MNPC,NCG),XH(MNPC,NCG),NPC(4)
        COMMON/CRV/Y(101,X(101,NCURVE
        DATA (NCURVE=0)
        SY=100./((YL-YS)/8.)
        SX=100./((XL-XS)/8.)
        CALL PLOT (YS,XS,0,SY,SX)
        DO 25 NC=1,NCG
        NCURVE=NCURVE+1
        K=NPC(NC)
        DO 3 J=1,K
        Y(J)=YV(J,NC)
     3  X(J)=XH(J,NC)
        IF (K.GE.101) GO TO 9
        DO 5 I=1,K
        CALL SYMBOL (NC,Y(I),X(I),SY,SX)
     5   CONTINUE
        K=NPC(NC)-LP+1
        CALL LSTSQ (K,XL,XS,LP)
     9  DO 10 I=1,101
        IF (Y(I).GT.YL-0.005) Y(I)=YL
        IF (Y(I).LT.YS+0.005 Y(I)=YS
```

```
 10 CONTINUE
 15  CALL PLOT (Y(1),X(1),2,SY,SX)
    IF (Y(1).NE.YS.AND.Y(1).NE.YL) CALL SYMBOL (NC,Y(1),
                          X(1),XY,SX)
    NP=K
    IF (K.LT.101)  NP=101
    DO 20 I=2,NP $ J1=1
    I1=I+1 $ IM1=I-1
    YT1=(Y(I)=YS)*(YL-Y(I)) $ YT2=(YIM1)-YS)*(YL-Y(IM1))
    IF (YT1.EQ.0.0.AND,TY2.EQ.0.0) J1=2
    CALL PLOT (Y(I), X(I),X(I),J1,SY,SX)
    IF (YT1.EQ.0.0.AND.I.NE.NP) GO TO 17
    IF (YT1.NE.0.0.AND.I.EQ.NP) GO TO 10  $  GO TO 20
 17 IF (Y(IM1).EQ.YL.AND.Y(I1).LT.YL) GO TO 19
    IF (Y(IM1).LT.YL.AND.Y(L1).EQ.YL) GO TO 19
    IF (Y(IM1).GT.YS.AND.Y(I1).EQ.YS) GO TO 19
    IF (Y(IM1).EQ.YS.AND.Y(I1).GT.YS) GO TO 10  $ GO TO 20
 19 CALL SYMBOL (NC,Y(I),X(I),SY,SX)
 20 CONTINUE
 25 CONTINUE
    CALL PLOT (YS,XS,2,SY,SX)


    SUBROUTINE LSTSQ (K,XL,XS,LP)
    DIMENSION W (101), R(2,101),C(10)
    COMMON/CRV/Y(101),X(101),NCURVE
    COMMON/GRA/N
    PRINT 100
100 FORMAT (13H1LSTSQ OUTPUT,//)
    K=K+LP-1
    DO 5 I=1,K
  5 W(I)+1.0
    KP=K-LP+1
    CALL MCPALS (KP,N,0.0.W,X,Y,R,C,LP,IDEG)
    PRINT 105, NCURVE,(I,R(1,I),R(2,I),I=LP,K)
105 FORMAT (4X,*CURVE NO.*,I3,/,42X,5HERROR,15X,10HFRAC ERROR,
                          //
   A       (38X,I3,X,2(E12.4,8X)))
    IDEG1=IDEG+1
    PRINT 110, IDEG,(C(I),I=1,IDGE1)
110  FORMAT (//,X,*IDEG=*,I2,/,X,*LSTSQ COEF*,/,(X,5
                         (E16.8,X)))
    DO 10 J=1,101
    X(J)=(J-1)*0.01*(XL-XS)+XS $ Y(J)=0.0
    IF (X(J).EQ.0.0) GO TO 9
    DO 8 I=1,IDEG1
    Y(J)=Y(J)+C(I)*X(J)**(I-1)
  8  CONTINUE $ GO TO 10
  9  Y(J)=C(1)
 10  CONTINUE
    END
```

```
   SUBROUTINE SYMBOL (NC,YI,XI,SY,SX)
   R=0.04
   CALL PLOT (YI,XI,2,SY,SX)
   GO TO (1,2,3,4),NC
 1 CALL CIRCLE (R,RI,XI)   $  GO TO 5
 2 CALL TRI (R,YI,XI)      $  GO TO 5
 3 CALL SQU (R,YI,XI)      $  GO TO 5
 4 CALL DIA (R,YI,XI)
 5 CALL PLOT (YI,XI,1,SY,SX)
   END

   SUBROUTING CIRCLE (R,YI,XI)
   CALL PLOT (YI,XI,2,100.,100.)
   CALL PLOT (YI,XI+R,2)
   DO 12 I=10,360,10
   A=I*3,1415926536/180.
   X=R*COSF(A)+XI  $  Y=R*SINF(A)+YI
   CALL PLOT (Y,X,1)
12 CONTINUE
   CALL PLOT (YI,XI,2)
   END


   SUBROUTINE TRI (R,YI,XI)
   CALL PLOT (YI,XI,2,100.,100.)
   CALL PLOT (-(2./3.)*0.866*R+YI,XI+R,2)
   CALL PLOT ((4./3.)*0.866*R+YI,XI,1)
   CALL PLOT (-(2./3.)*0.866*R+YI,XI-R,1)
   CALL PLOT (-(2./3.)*0.866*R+YI,XI+R,1)
   CALL PLOT (YI,XI,2)
   END


   SUBROUTINE SQU (R,YI,XI)
   CALL PLOT (YI,XI,2,100.,100.)
   CALL PLOT YI-R,XI+R,2)
   CALL PLOT (YI+R,XI+R,1)
   CALL PLOT (YI+R,XI-R,1)
   CALL PLOT (YI-R,XI-R,1)
   CALL PLOT (YI-R,XI+R,1)
   CALL PLOT (YI,XI,2)
   END


   SUBROUTINE DIA (R,YI,XI)
   CALL PLOT (YI,XI,2,100.,100.)
   CALL PLOT (YI,XI+R,2)
```

```
      CALL PLOT (YI+R,XI,1)
      CALL PLOT (YI,XI-R,1)
      CALL PLOT (YI-R,XI,1)
      CALL PLOT (YI,XI+R,1)
      CALL PLOT (YI,XI,2)
      END


      SUBROUTINE MCPALS(M,N,EPS,W,X,Y,R,C,LP,IDEG)
         DIMENSION W(M),X(M),Y(M),A(10,10),SUMXSQ(19),
                                 C(10),R(2,M),B(10)
         SUMXSQ(1)=B(1)=0
         NMX=N
         IF((M-N-1).LT.0) NMX=M-1
         NMX1=NMX+1
      MN=M+LP-1
         DO 1 I=LP,MN
            R(2,I)=1.0
            B(1)=B(1)+Y(I)+W(I)
    1       SUMXSQ(1)=SUMXSQ(1)+W(I)
         R(1,1)=B(1)
         NMN=1
         IF(EPS.EQ.0) NMN=NMX
         DO 10 NN=NMN,NMX
            N2=2*NN
            N1-NN+1
            N21=N2-1
            IF(EPS.EQ.0) N21=1
            DO 2 J=N21,N2
               J1=J+1
               IF(J1.LE.NMX1) B(J1)=0
               SUMXSQ(J1)=0
         DO 2 I=LP,MN
                  R(2,I)=R(2,I)*X(I)
                  SUM=R(2,I)*W(I)
                  IF(J1.LE.NMX1) R(1,J1)=B(J1)=B(J1)+SUM*Y(I)
    2             SUMXSQ(J1)=SUMXSQ(J1)+SUM
            DO 3 I=1,N1
               J1=I-1
               DO 3 J=1,N1
    3             A(I,J)=SUMXSQ(J1+J)
            CALL GAUSS (N1,A,B,C)
            DO 4 I=1,N1
    4          B(I)+R(1,I)
         DO 8 I=LP,MN
               SUM=C(N1)
               DO 5 J=1,NN
    5             SUM=X(I)*SUM+C(N1-J)
               SUM=Y(I)-SUM
               IF((ABSF(SUM).LT.EPS).OR.(NN.EQ.NMX))GO TO 7
```

```
            DO 6 J=1,NMX1
  6            R(1,J)=B(J)
            GO TO 10
  7         R(1,I)=SUM
  8         CONTINUE
      DO 9 I=LP,MN
  9          R(2,I)=R(1,I)/Y(I)
         IDEG=NN
         RETURN
 10    CONTINUE
       RETURN
     END


     SUBROUTING GAUSS(M,A,B,C)
        DIMENSION A(10,10),B(M),C(M)
101     FORMAT (//53X,30H***SINGULAR MATRIX IN GAUSS***//)
        DO 6 K=1,M
           C(1)=0
           IMAX=K
           DO 1 I=K,M
              T=ABSF(A(1,K))
           IF(C(1).GE.T) GO TO 1
              C(1)=T
              1 MAX=I
  1           CONTINUE
           IF(C(1).NE.0) GO TO 2
              PRINT 101
              RETURN
  2        IF(K.EQ.IMAX) GO TO 4
              J=IMAX
              T=B(K)
              B(K)=B(J)
              B(J)=T
              DO 3 L=1,M
                 T=A(K,L)
                 A(K,L)=A(J,L)
  3              A(J,L)=T
  4        I=K+1
           DO 5 J=I,M
              T=A(J,K)/A(K,K)
              B(J)+B(J)-B(K)*T
              DO 5 L=I,M
   5             A(J,L)=A(J,L)-T*A(K,L)
   6       CONTINUE
           J=M+1
           DO 8 K=1,M
              I=J-K
              T=0
              IMAX=I+1
              DO 7 L=IMAX,M
```

```
7              T=T+A(I,L)*C(L)
8           C(I)=(B(I)-T)/A(I,I)
         RETURN
       END
```